Advanced Course and Workshop on Blood Flow
BF 2005 – (pp.31–90) – Warsaw, 2005.

Pressure and Flow in the Cardiovascular System

Frans N. van de Vosse

Department of Biomedical Engineering
Eindhoven University of Technology
The Netherlands

In the introductory part of these notes a short overview of the circulatory system with respect to blood flow and pressure will be given. In section 1 a simple model of the vascular system will be presented despite the fact that the fluid mechanics of the cardiovascular system is complex due to the non-linear and non-homogeneous rheological properties of blood and arterial wall, the complex geometry and the pulsatile flow properties.
An important part, section 2, is dedicated to the description of Newtonian flow in straight, curved and bifurcating, rigid tubes. With the aid of characteristic dimensionless parameters the flow phenomena will be classified and related to specific physiological phenomena in the cardiovascular system. In this way difference between flow in the large arteries and flow in the micro-circulation and veins and the difference between flow in straight and curved arteries will be elucidated. It will be shown that the flow in branched tubes shows a strong resemblance to the flow in curved tubes.
Although flow patterns as derived from rigid tube models do give a good approximation of those that can be found in the vascular system, they will not provide information on pressure pulses and wall motion. In order to obtain this information a short introduction to vessel wall mechanics will be given and models for wall motion of distensible tubes as a function of a time dependent pressure load will be derived. The flow in distensible tubes is determined by wave propagation of the pressure pulse. The main characteristics of the wave propagation including attenuation and reflection of waves at geometrical transitions are treated in section 3, using a one-dimensional wave propagation model.

Key words: *hemodynamics, curved tube flow, vascular biomechanics, wave propagation, wave reflection*

1. The Cardiovascular System

1.1. Introduction

The study of cardiovascular fluid mechanics is only possible with some knowledge of cardiovascular physiology. In this section a brief introduction to cardiovascular physiology will be given. Some general aspects of the fluid mechanics of the heart, the arterial system, the micro-circulation and the venous system as well as the most important properties of the vascular tree that determine the pressure and flow characteristics in the cardiovascular system will be dealt with. Although the fluid mechanics of the vascular system is complex due to complexity of geometry and pulsatility of the flow, a simple linear model of this system will be derived.

1.2. Short Overview of the Cardiovascular System

The cardiovascular system takes care of convective transport of blood between the organs of the mammalian body in order to enable diffusive transport of oxygen, carbon oxide, nutrients and other solutes at cellular level in the tissues. Without this convective transport an appropriate exchange of these solutes would be impossible because of a too large diffusional resistance. An extended overview of physiological processes that are enabled by virtue of the cardiovascular system can be found in standard text books on physiology like [3].

The circulatory system can be divided into two parts in series, the pulmonary circulation and the systemic circulation (see Fig. 1). Blood received by the right atrium (RA) from the venae cavae is pumped from the right ventricle (RV) of the heart into the pulmonary artery which strongly bifurcates in pulmonary arterioles transporting the blood to the lungs. The left atrium (LA) receives the oxygenated blood back from the pulmonary veins. Then the blood is pumped via the left ventricle (LV) into the systemic circulation. As from fluid mechanical point of view the main flow phenomena in the pulmonary circulation match the phenomena in the systemic circulation, in the sequel of this course only the systemic circulation will be considered.

1.2.1. The heart. The forces needed for the motion of the blood are provided by the heart, which serves as a four-chambered pump that propels blood around the circulatory system (see Fig. 1). Since the mean pressure in

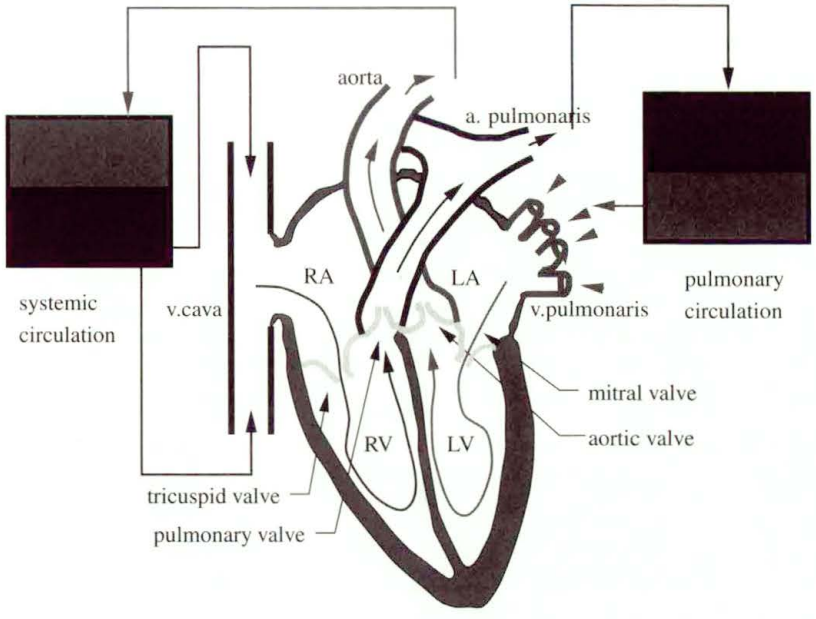

FIGURE 1. Schematic representation of the heart and the circulatory system. RA = right atrium, LA = left atrium, RV = right ventricle, LV = left ventricle.

the systemic circulation is approximately 13 kPa, which is more than three times the pressure in the pulmonary system (≈ 4 kPa), the thickness of the left ventricular muscle is much larger then that of the right ventricle.

The ventricular and aortic pressure and aortic flow during the cardiac cycle are given in Fig. 2. Atrial contraction, induced by a stimulus for muscle contraction of the sinoatrial node, causes a filling of the ventricles with hardly any increase of the ventricular pressure. In the left heart the mitral valve is opened and offers very low resistance. The aortic valve is closed. Shortly after this, at the onset of systole the two ventricles contract simultaneously controlled by a stimulus generated by the atrioventricular node. At the same time the mitral valve closes (mc) and a sharp pressure rise in the left ventricle occurs. At the moment that this ventricular pressure exceeds the pressure in the aorta, the aortic valve opens (ao) and blood is ejected into the aorta. The ventricular and aortic pressure first rise and then fall as a result of a combined action of ventricular contraction forces and the resistance and compliance of the systemic circulation. Due to this pressure fall (or actually the corresponding flow deceleration) the aortic valve closes (ac) and the pressure in the ventricle drops rapidly, the mitral valve opens (mo), while the heart muscle relaxes (diastole).

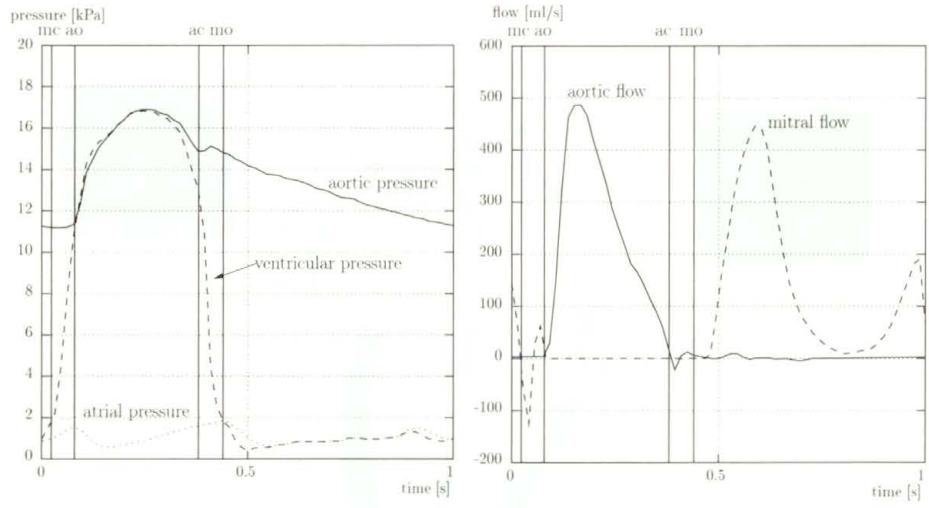

FIGURE 2. Pressure in the left atrium, left ventricle and the aorta (left) and flow through the mitral valve and the aorta (right) as a function of time during one cardiac cycle, after [4]. With times: mc = mitral valve closes, ao = aortic valve opens, ac = aortic valve closes and mo = mitral valve opens.

Since, in the heart, both the blood flow velocities as well as the geometrical length scales are relatively large, the fluid mechanics of the heart is strongly determined by inertial forces which are in equilibrium with pressure forces.

1.2.2. The systemic circulation. The systemic circulation can be divided into three parts: the arterial system, the capillary system and the venous system. The main characteristics of the systemic circulation are depicted schematically in Fig. 3.

From Fig. 3 it can be seen that the diameter of the blood vessels strongly decrease from the order of 0.5–20 mm in the arterial system to 5–500 μm in the capillary system. The diameters of the vessels in the venous system in general are slightly larger then those in the arterial system. The length of the vessels also strongly decreases and increases going from the arterial system to the venous system but only changes in two decades. Most dramatic changes can be found in the number of vessels that belong to the different compartments of the vascular system. The number of vessels in the capillary system is of order $O(10^6)$ larger then in the arterial and venous system. As a consequence, the total cross section in the capillary system is about 1000 times larger then in the arterial and the venous system, enabling an

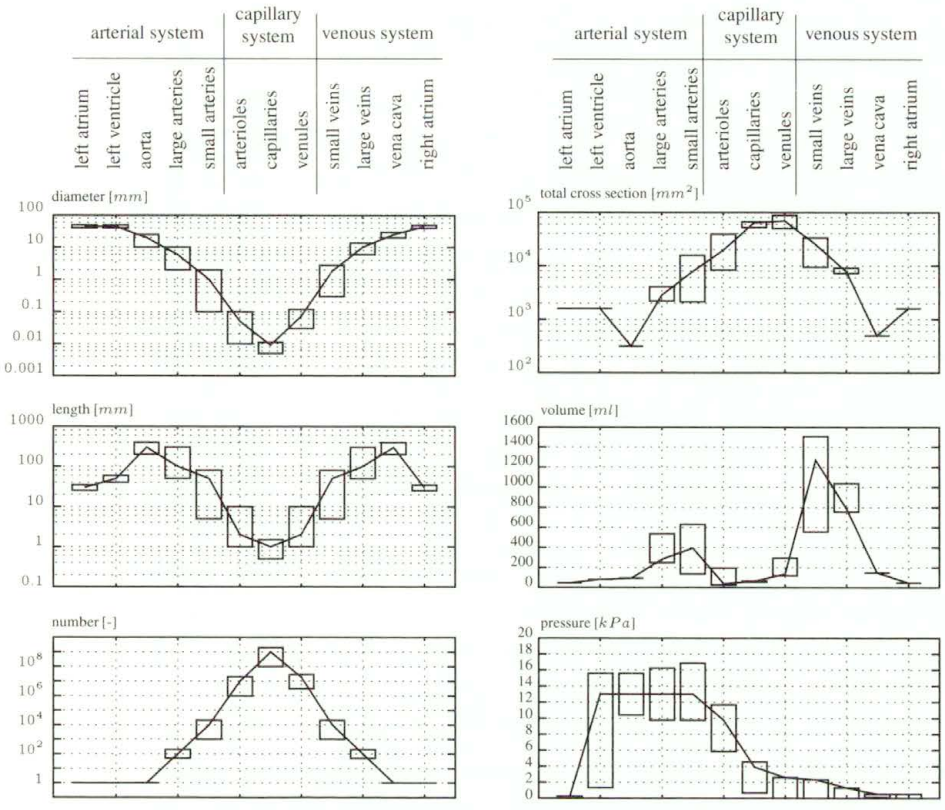

FIGURE 3. Rough estimates of the diameter, length and number of vessels, their total cross-section and volume and the pressure in the vascular system.

efficient exchange of solutes in the tissues by diffusion. Combination of the different dimensions mentioned above shows that the total volume of the venous system is about 2 times larger then the volume of the arterial system and much larger then the total volume of the capillary system. As can be seen from the last figure, the mean pressure falls gradually as blood flows into the systemic circulation. The pressure amplitude, however, shows a slight increase in the proximal part of the arterial system.

The *arterial system* is responsible for the transport of blood to the tissues. Besides the transport function of the arterial system the pulsating flow produced by the heart is also transformed to a more-or-less steady flow in the smaller arteries. Another important function of the arterial system is to maintain a relatively high arterial pressure. This is of importance for a proper functioning of the brain and kidneys. This pressure can be kept

at this relatively high value because the distal end of the arterial system strongly bifurcates into vessels with small diameters (arterioles) and hereby forms a large peripheral resistance. The smooth muscle cells in the walls are able to change the diameter and hereby the resistance of the arterioles. In this way the circulatory system can adopt the blood flow to specific parts in accordance to momentary needs (vasoconstriction and vasodilatation). Normally the heart pumps about 5 liters of blood per minute but during exercise the heart minute volume can increase to 25 liters. This is partly achieved by an increase of the heart frequency but is mainly made possible by local regulation of blood flow by vasoconstriction and vasodilatation of the distal arteries (arterioles). Unlike the situation in the heart, in the arterial system, also viscous forces may become of significant importance as a result of a decrease in characteristic velocity and length scales (diameters of the arteries).

Leaving the arterioles the blood flows into the *capillary system*, a network of small vessels. The walls consist of a single layer of endothelial cells lying on a basement membrane. Here an exchange of nutrients with the interstitial liquid in the tissues takes place. In physiology, capillary blood flow is mostly referred to as micro circulation. The diameter of the capillaries is so small that the whole blood may not be considered as a homogeneous fluid anymore. The blood cells are moving in a single file (train) and strongly deform. The plasma acts as a lubrication layer. The fluid mechanics of the capillary system hereby strongly differs from that of the arterial system and viscous forces dominate over inertia forces in their equilibrium with the driving pressure forces.

Finally the blood is collected in the *venous system* (venules and veins) in which the vessels rapidly merge into larger vessels transporting the blood back to the heart. The total volume of the venous system is much larger then the volume of the arterial system. The venous system provides a storage function which can be controlled by constriction of the veins (venoconstriction) that enables the heart to increase the arterial blood volume. As the diameters in the venous system are of the same order of magnitude as in the arterial system, inertia forces may become influential again. Both characteristic velocities and pressure amplitudes, however, are lower than in the arterial system. As a consequence, in the venous system, instationary inertia forces will be of less importance then in the arterial system. Moreover, the pressure in the venous system is that low that gravitational forces become of importance.

The geometrical dimensions referred to above and summarized in Fig. 3 show that the vascular tree is highly bifurcating and will be geometrically complex. Flow phenomena related with curvature and bifurcation of the vessels (see Sec. 2) can not be neglected. As in many cases the length of the vessels is small compared to the length needed for fully developed flow, also entrance flow must be included in studies of cardiovascular fluid mechanics.

1.3. Pressure and Flow in the Cardiovascular System

1.3.1. Pressure and flow waves in arteries. The pressure in the aorta significantly changes with increasing distance from the heart. The peak of the pressure pulse delays downstream indicating wave propagation along the aorta with a certain wave speed. Moreover, the shape of the pressure pulse changes and shows an increase in amplitude, a steepening of the front and only a moderate fall of the mean pressure (see Fig. 4).

This wave phenomenon is a direct consequence of the distensibility of the arterial wall, allowing a partial storage of the blood injected from the heart due to an increase of the pressure and the elastic response of the vessel walls. The cross-sectional area of the vessels depends on the pressure difference

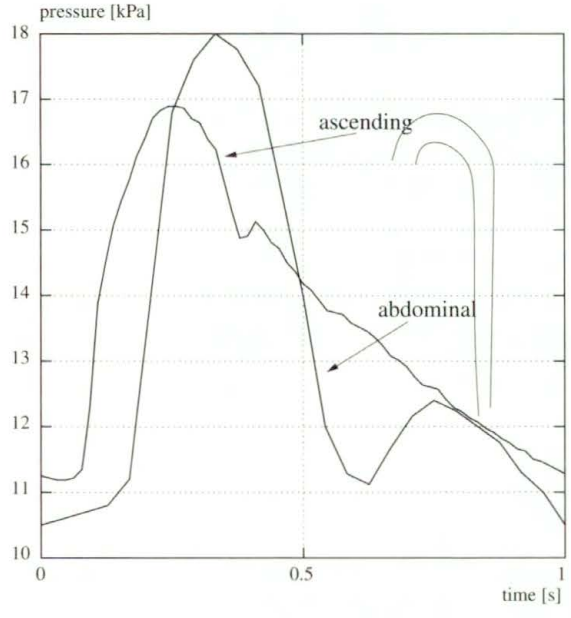

FIGURE 4. Typical pressure waves at two different sites in the aorta

over the wall. This pressure difference is called the transmural pressure and is denoted by p_{tr}. This transmural pressure consists of several parts. First, there exists a hydrostatic part proportional to the density of the blood inside ρ, the gravity force g and the height h. This hydrostatic part is a result of the fact that the pressure outside the vessels is closely to atmospheric. Next, the pressure is composed of a time independent part p_0 and a periodic, time dependent part p. So the transmural pressure can be written as:

$$p_{tr} = \rho g h + p_0 + p. \tag{1.1}$$

Due to the complex nonlinear anisotropic and viscoelastic properties of the arterial wall, the relation between the transmural pressure and the cross sectional area A of the vessel is mostly nonlinear and can be rather complicated. Moreover it varies from one vessel to the other. Important quantities with respect to this relation, used in physiology, are the compliance or alternatively the distensibility of the vessel. The compliance C is defined as:

$$C = \frac{\partial A}{\partial p}. \tag{1.2}$$

For thin wall tubes the following relation can be derived:

$$C = \frac{\partial A}{\partial p} = \frac{2\pi a_0^3}{h} \frac{(1-\mu^2)}{E}. \tag{1.3}$$

The distensibility D is defined by the ratio of the compliance and the cross sectional area and hereby is given by:

$$D = \frac{1}{A} \frac{\partial A}{\partial p} = \frac{C}{A}. \tag{1.4}$$

In the sequel of this course these quantities will be related to the material properties of the arterial wall. For thin walled tubes, with radius a and wall thickness h, without longitudinal strain, e.g., it can be derived that:

$$D = \frac{2a}{h} \frac{1-\mu^2}{E}. \tag{1.5}$$

Here μ denotes Poisson 's ratio and E Young's modulus. From this we can see that besides the properties of the material of the vessel (E, μ) also geometrical properties (a, h) play an important role.

The value of the ratio a/h varies strongly along the arterial tree. The veins are more distensible than the arteries. Mostly, in some way, the pressure-area

relationship, i.e. the compliance or distensibility, of the arteries or veins that are considered, have to be determined from experimental data. A typical example of such data is given in Fig. 5 where the relative transmural pressure p/p_0 is given as a function of the relative cross-sectional area A/A_0. As depicted in this figure, the compliance changes with the pressure load since at relatively high transmural pressure, the collagen fibres in the vessel wall become streched and prevent the artery from further increase of the circumferential strain.

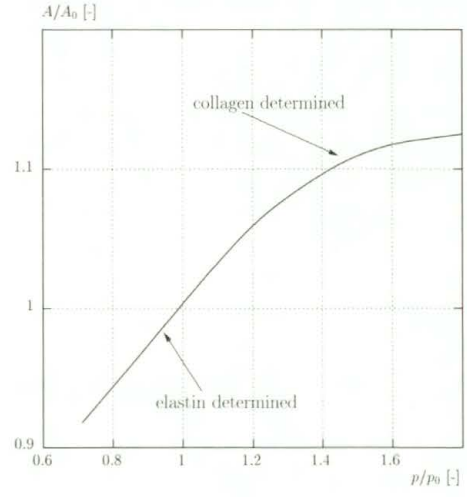

FIGURE 5. Typical relation between the relative transmural pressure p/p_0 and the relative cross-sectional area A/A_0 of an artery.

The flow is driven by the gradient of the pressure and hereby determined by the propagation of the pressure wave. Normally the pressure wave will have a pulsating periodic character. In order to describe the flow phenomena we distinguish between steady and unsteady part of this pulse. Often it is assumed that the unsteady part can be described by means of a linear theory, so that we can introduce the concept of pressure and flow waves which be superpositions of several harmonics:

$$p = \sum_{n=1}^{N} p_n e^{ni\omega t} \qquad q = \sum_{n=1}^{N} q_n e^{ni\omega t} \tag{1.6}$$

Here p_n and q_n are the complex Fourier coefficients and hereby p and q are the complex pressure and the complex flow, ω denotes the angular frequency of the basic harmonic. Actual pressure and flow can be obtained by taking

the real part of these complex functions. Normally spoken 6 to 10 harmonics are sufficient to describe the most important features of the pressure wave. Table 1 is adopted from [4] and represents the modulus and phase of the first 10 harmonics of the pressure and flow in the aorta. The corresponding pressure and flow are given in Fig. 6.

TABLE 1. First 10 harmonics of the pressure and flow in the aorta, from [4].

	q in ml/s		p in mm Hg	
harmonic	modulus	phase	modulus	phase
0	110	0	85	0
1	202	-0.78	18.6	-1.67
2	157	-1.50	8.6	-2.25
3	103	-2.11	5.1	-2.61
4	62	-2.46	2.9	-3.12
5	47	-2.59	1.3	-2.91
6	42	-2.91	1.4	-2.81
7	31	+2.92	1.2	+2.93
8	19	+2.66	0.4	-2.54
9	15	+2.73	0.6	-2.87
10	15	+2.42	0.6	+2.87

1.3.2. Pressure and flow in the micro-circulation. The micro-circulation is a strongly bifurcating network of small vessels and is responsible for the exchange of nutrients and gases between the blood and the tissues. Mostly blood can leave the arterioles in two ways. The first way is to follow a metarteriole towards a specific part of the tissue and enter the capillary system. This second way is to bypass the tissue by entering an arterio venous anastomosis that shortcuts the arterioles and the venules. Smooth muscle cells in the walls of the metarterioles, precapillary sphincters at the entrance of the capillaries and glomus bodies in the anastomoses regulate the local distribution of the flow. In contrast with the arteries the pressure in the micro-vessels is more or less constant in time yielding an almost steady flow. This steadiness, however, is strongly disturbed by the 'control actions' of the regulatory system of the micro-circulation. As the dimensions of the blood cells are of the same order as the diameter of the micro-vessels the flow and deformation properties of the red cells must be taken into account in the modeling of the flow in the micro-circulation (see Sec. 2).

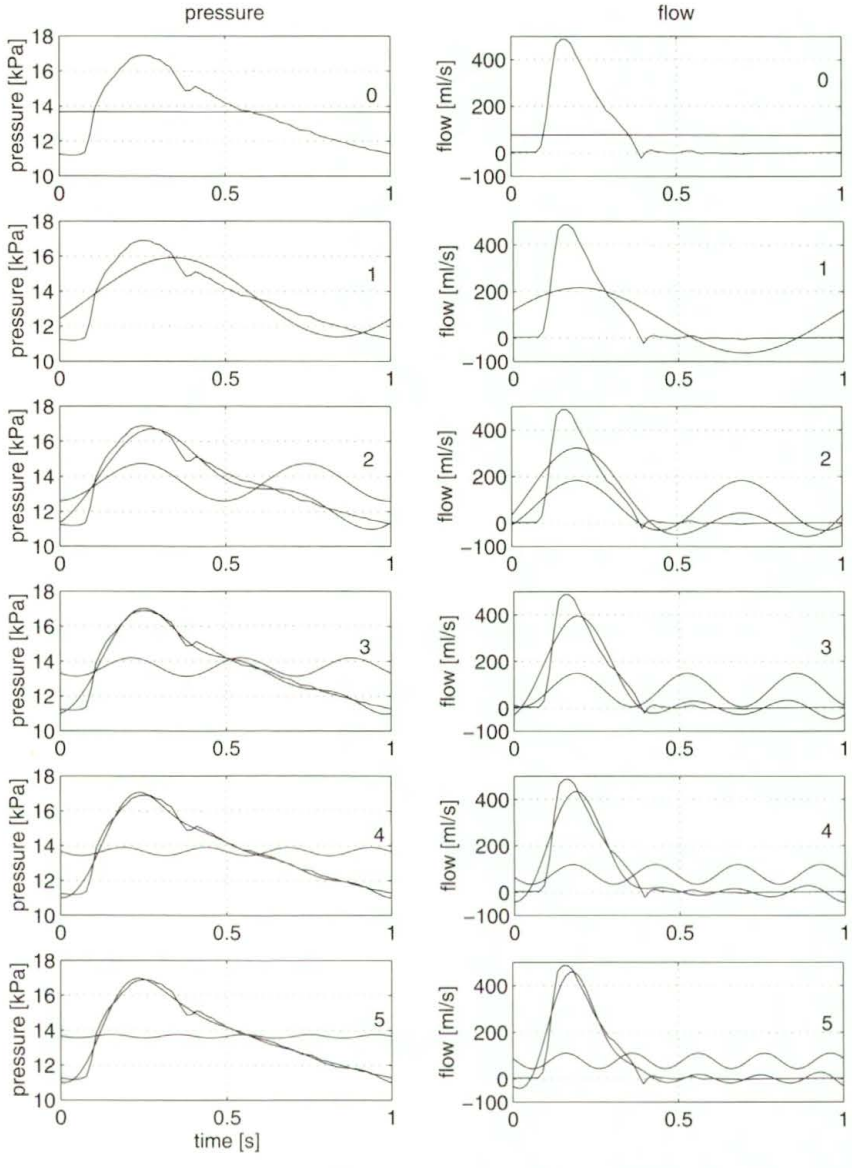

FIGURE 6. Pressure and flow in the aorta based on the data given in Table 1

1.3.3. Pressure and flow in the venous system. The morphology of the systemic veins resemble arteries. The wall however is not as thick as in the arteries of the same diameter. Also the pressure in a vein is much lower than the pressure in an artery of the same size. In certain situations the pressure can be so low that in normal functioning the vein will have an elliptic cross-sectional area or even will be collapsed for some time. Apart from its different wall thickness and the relatively low pressures, the veins distinguish from arteries by the presence of valves to prevent back flow.

1.4. Simple Model of the Vascular System

1.4.1. Periodic deformation and flow. In cardiovascular fluid dynamics the flow often may be considered as periodic if we assume a constant duration of each cardiac cycle. In many cases, i.e. if the deformation and the flow can be described by a linear theory, the displacements and velocity can be decomposed in a number of harmonics using a Fourier transform:

$$v = \sum_{n=0}^{N} \hat{v}_n e^{in\omega t}. \tag{1.7}$$

Here $\hat{v}_n$ are the complex Fourier coefficients, ω denotes the angular frequency of the basic harmonic. Note that a complex notation of the velocity is used exploiting the relation:

$$e^{i\omega t} = \cos(\omega t) + i \sin(\omega t) \tag{1.8}$$

with $i = \sqrt{-1}$. The actual velocity can be obtained by taking the real part of the complex velocity. By substitution of relation (1.7) in the governing equations that describe the flow, often an analytical solution can be derived for each harmonic. Superposition of these solution then will give a solution for any periodic flow as long as the equations are linear in the solution v.

1.4.2. The windkessel model. Incorporating some of the physiological properties described above several models for the cardiovascular system has been derived in the past. The most simple model is the one that is known as the *windkessel* model. In this model the aorta is represented by a simple compliance C (elastic chamber) and the peripheral blood vessels are assumed to behave as a rigid tube with a constant resistance (R_p) (see top of Fig. 7).

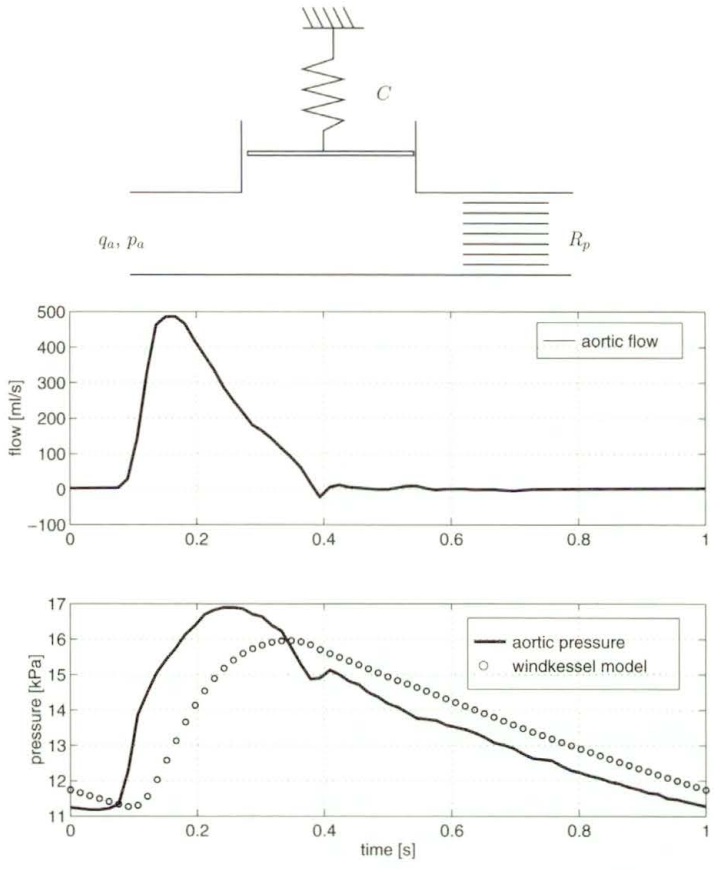

FIGURE 7. Windkessel model of the cardiovascular system (top). Aortic flow and pressure, data from [4] as function of time with pressure obtained from the windkessel model indicated with the dotted line (bottom).

The pressure p_a in the aorta as a function of the left ventricular flow q_a then is given by:

$$q_a = C\frac{\partial p_a}{\partial t} + \frac{p_a}{R_p} \tag{1.9}$$

or after Fourier transformation:

$$\hat{q}_a = (i\omega C + \frac{1}{R_p})\hat{p}_a. \tag{1.10}$$

In the bottom two charts of Fig. 7 experimental data [4] of the flow in the aorta (upper chart) is plotted as a function of time. This flow is used as input for the computation of the pressure from Eq. (1.9) and compared with experimental data (dotted resp. solid line in Fig. 7). The resistance R_p

and compliance C were obtained from a least square fit and turned out to be $R_p = 0.18\,\text{kPa·s/ml}$ and $C = 11.5\,\text{ml/kPa}$.

During the diastolic phase of the cardiac cycle the aortic flow is relatively low and Eq. (1.9) can be approximated by:

$$\frac{\partial p_a}{\partial t} \approx \frac{1}{R_p C} p_a \qquad \text{during diastole} \tag{1.11}$$

with solution $p_a \approx p_{as} e^{-t/R_p C}$ with p_{as} peak systolic pressure. This approximate solution resonably corresponds with experimental data.

During the systolic phase of the flow the aortic flow is much larger then the peripheral flow ($q_a \gg p_a/R_p$) yielding:

$$\frac{\partial p_a}{\partial t} \approx \frac{1}{C} q_a \qquad \text{during systole} \tag{1.12}$$

with solution $p_a \approx p_{ad} + (1/C) \int q_a dt$ with p_{ad} the diastolic pressure. Consequently a phase difference between pressure and flow is expected. Experimental data, however, show $p_a \approx p_{ad} + k q_a$, so pressure and flow are more or less in-phase (see Fig. 7). Notwithstanding the significant phase error in the systolic phase, this simple windkessel model is often used to derive the cardiac work at given flow. Note that for linear time-periodic systems, better fits can be obtained using the complex notation (1.10) with frequency dependent resistance ($R_p(\omega)$) and compliance $C(\omega)$).

In Sec. 3 of this course we will show that this model has strong limitations and is in contradiction with important features of the vascular system.

1.4.3. Vascular impedance. As mentioned before the flow of blood is driven by the force acting on the blood induced by the gradient of the pressure. The relation of these forces to the resulting motion of blood is expressed in the longitudinal impedance:

$$Z_L = \frac{\partial \hat{p}}{\partial z} / \hat{q}. \tag{1.13}$$

The longitudinal impedance is a complex number defined by complex pressures and complex flows. It can be calculated by frequency analysis of the pressure gradient and the flow that have been recorded simultaneously. As it expresses the flow induced by a local pressure gradient, it is a property of a small (infinitesimal) segment of the vascular system and depends on local properties of the vessel. The longitudinal impedance plays an important role in the characterization of vascular segments. It can be measured

by a simultaneous determination of the pulsatile pressure at two points in the vessel with a known small longitudinal distance apart from each other together with the pulsatile flow. In Sec. 3 the longitudinal impedance will be derived mathematically using a linear theory for pulsatile flow in rigid and distensible tubes. A second important quantity is the input impedance defined as the ratio of the pressure and the flow at a specific cross-section of the vessel:

$$Z_i = \hat{p}/\hat{q}. \tag{1.14}$$

The input impedance is not a local property of the vessel but a property of a specific site in the vascular system. If some input condition is imposed on a certain site in the system, than the input impedance only depends on the properties of the entire vascular tree distal to the cross-section where it is measured. In general the input impedance at a certain site depends on both the proximal and distal vascular tree. The compliance of an arterial segment is characterized by the transverse impedance defined by:

$$Z_T = \hat{p}/\frac{\partial \hat{q}}{\partial z} \approx -\hat{p}/i\omega\hat{A}. \tag{1.15}$$

This relation expresses the flow drop due to the storage of the vessel caused by the radial motion of its wall (A being the cross-sectional area) at a given pressure (note that $i\omega\hat{A}$ represents the partial time derivative $\partial A/\partial t$). In Sec. 3 it will be shown that the impedance-functions as defined here can be very useful in the analysis of wave propagation and reflection of pressure and flow pulses traveling through the arterial system.

2. Newtonian Flow in Blood Vessels

2.1. Steady and Pulsatile Newtonian Flow in Straight Tubes

In this section the flow patterns in rigid straight, curved and branching tubes will be considered. First, fully developed flow in straight tubes will be dealt with and it will be shown that this uni-axial flow is characterized by two dimensionless parameters, the Reynolds number Re and the Womersley number α, that distinguish between flow in large and small vessels. Also derived quantities, like wall shear stress and vascular impedance, can be expressed as a function of these parameters.

For smaller tube diameters (micro-circulation), however, the fluid can not be taken to be homogeneous anymore and the dimensions of the red blood

cells must be taken into account. In the entrance regions of straight tubes, the flow is more complicated. Estimates of the length of these regions will be derived for steady and pulsatile flow.

The flow in curved tubes is not uni-axial but exhibits secondary flow patterns perpendicular to the axis of the tube. The strength of this secondary flow field depends on the curvature of the tube which is expressed in another dimensionless parameter: the Dean number. Finally it will be shown that the flow in branched tubes shows a strong resemblance to the flow in curved tubes.

2.1.1. Fully Developed Flow

Governing equations

To analyze fully developed Newtonian flow in rigid tubes consider the Navier-Stokes equations in a cylindrical coordinate system:

$$\begin{cases} \dfrac{\partial v_r}{\partial t} + v_r\dfrac{\partial v_r}{\partial r} + v_z\dfrac{\partial v_r}{\partial z} = -\dfrac{1}{\rho}\dfrac{\partial p}{\partial r} + \nu\left(\dfrac{\partial}{\partial r}\left(\dfrac{1}{r}\dfrac{\partial}{\partial r}(rv_r)\right) + \dfrac{\partial^2 v_r}{\partial z^2}\right), \\ \dfrac{\partial v_z}{\partial t} + v_r\dfrac{\partial v_z}{\partial r} + v_z\dfrac{\partial v_z}{\partial z} = -\dfrac{1}{\rho}\dfrac{\partial p}{\partial z} + \nu\left(\dfrac{1}{r}\dfrac{\partial}{\partial r}\left(r\dfrac{\partial}{\partial r}(v_z)\right) + \dfrac{\partial^2 v_z}{\partial z^2}\right), \\ \dfrac{1}{r}\dfrac{\partial}{\partial r}(rv_r) + \dfrac{\partial v_z}{\partial z} = 0. \end{cases} \tag{2.1}$$

Since the velocity in circumferential direction equals zero ($v_\phi = 0$), the momentum equation and all derivatives in ϕ-direction are omitted. For fully developed flow the derivatives of the velocity in axial direction $\frac{\partial}{\partial z}$ and the velocity component in radial direction v_r are zero and Eqs. (2.1) simplify to:

$$\frac{\partial v_z}{\partial t} = -\frac{1}{\rho}\frac{\partial p}{\partial z} + \frac{\nu}{r}\frac{\partial}{\partial r}\left(r\frac{\partial v_z}{\partial r}\right). \tag{2.2}$$

Now a dimensionless velocity can be defined as $v_z^* = v_z/V$, the coordinates can be made dimensionless using the radius of the tube, i.e. $r^* = r/a$ and $z^* = z/a$, the pressure can be scaled as $p^* = p/\rho V^2$ and the time can be scaled using $t^* = \omega t$. Dropping the asterisk, the equation of motion reads:

$$\alpha^2\frac{\partial v_z}{\partial t} = -\mathrm{Re}\frac{\partial p}{\partial z} + \frac{1}{r}\frac{\partial}{\partial r}\left(r\frac{\partial v_z}{\partial r}\right) \tag{2.3}$$

with Re the Reynolds number given by

$$\mathrm{Re} = \frac{aV}{\nu} \tag{2.4}$$

and α the Womersley number defined as:

$$\alpha = a\sqrt{\frac{\omega}{\nu}}. \tag{2.5}$$

So two dimensionless parameters are involved: the Womersley number α defining the ratio of the non-stationary inertia forces and the viscous forces and the Reynolds number Re that is in this case nothing more then a scaling factor for the pressure gradient. The pressure could also be scaled according to $p^* = p/(a^2/\eta V)$ yielding one single parameter α.

In Table 2 the Womersley numbers for several sites in the arterial system are given. These values show that in the aorta and in the largest arteries inertia dominated flow and in arterioles and capillaries friction dominated flow may be expected. In most part of the arteries an intermediate value of α is found and both inertia and viscous friction are important.

TABLE 2. Estimated Womersley number at several sites of the arterial system based on the first harmonic of the flow. A kinematic viscosity of 5×10^{-3} Pa·s, a density of 10^3 kg·m^{-3} and a frequency of 1 Hz are assumed.

	a [mm]	α [–]
aorta	10	10
large arteries	4	4
small arteries	1	1
arterioles	0.1	0.1
capillaries	0.01	0.01

For the venous system a similar dependence of the Womersley number is found but it must be noted that inertia is less important due to the low amplitude of the first and higher harmonics with respect to the mean flow.

Velocity profiles

For flow in a rigid tube (see Fig. 8) with radius a the boundary condition $v(a,t) = 0$ is used to impose a no slip condition.

We will assume a harmonic pressure gradient and will search for harmonic solutions:

$$\frac{\partial p}{\partial z} = \frac{\partial \hat{p}}{\partial z} e^{i\omega t} \tag{2.6}$$

and

$$v_z = \hat{v}_z(r) e^{i\omega t}. \tag{2.7}$$

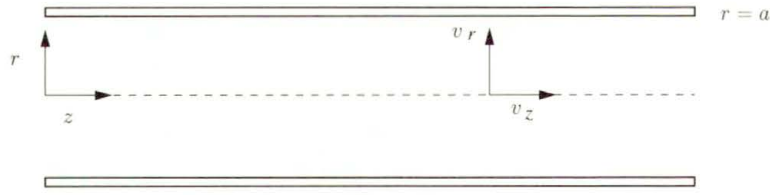

FIGURE 8. Rigid tube with radius a

The solution of an arbitrary periodic function then can be constructed by superposition of its harmonics. This is allowed because the equation to solve (2.3) is linear in v_z.

Now two asymptotic cases can be defined. For small Womersley numbers there is an equilibrium of viscous forces and the driving pressure gradient. For large Womersley numbers, however, the viscous forces are small compared to the instationary inertia forces and there will be an equilibrium between the inertia forces and the driving pressure gradient. Both cases will be considered in more detail.

Small Womersley number flow. If $\alpha \ll 1$ Eq. (2.3) (again in dimension-full form) yields:

$$0 = -\frac{1}{\rho}\frac{\partial p}{\partial z} + \frac{\nu}{r}\frac{\partial}{\partial r}\left(r\frac{\partial v_z}{\partial r}\right). \tag{2.8}$$

Substitution of Eq. (2.6) and (2.7) yields:

$$\nu\frac{\partial^2 \hat{v}_z(r)}{\partial r^2} + \frac{\nu}{r}\frac{\partial \hat{v}_z(r)}{\partial r} = \frac{1}{\rho}\frac{\partial \hat{p}}{\partial z} \tag{2.9}$$

with solution:

$$v_z(r,t) = -\frac{1}{4\eta}\frac{\partial \hat{p}}{\partial z}(a^2 - r^2)e^{i\omega t}. \tag{2.10}$$

So, for low values of the Womersley number a quasi-static Poiseuille profile is found. It oscillates 180° out of phase with the pressure gradient. The shape of the velocity profiles is depicted in the left graph of Fig. 9.

Large Womersley number flow. If the $\alpha \gg 1$ Eq. (2.3) yields:

$$\frac{\partial v_z}{\partial t} = -\frac{1}{\rho}\frac{\partial p}{\partial z}. \tag{2.11}$$

Substitution of Eq. (2.6) and (2.7) yields:

$$i\omega\hat{v}_z(r) = -\frac{1}{\rho}\frac{\partial \hat{p}}{\partial z} \tag{2.12}$$

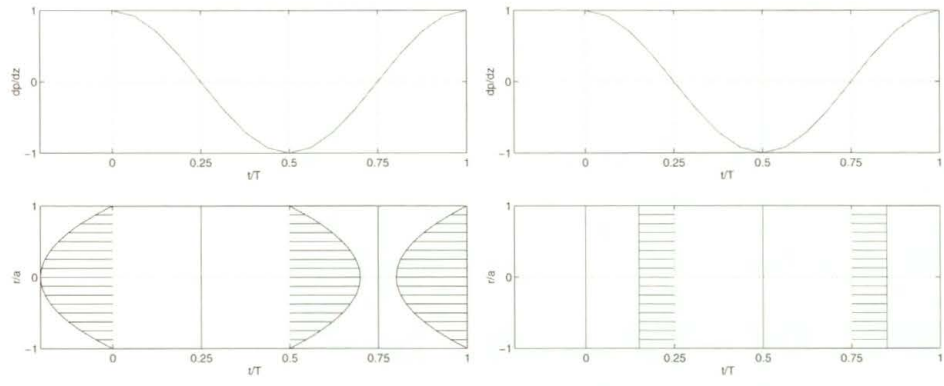

FIGURE 9. Pressure gradient (top) and corresponding velocity profiles (bottom) as a function of time for small (left) and large (right) Womersley numbers.

with solution:

$$v_z(r,t) = \frac{i}{\rho\omega}\frac{\partial \hat{p}}{\partial z}e^{i\omega t}. \tag{2.13}$$

Now, for high values of the Womersley number, an oscillating plug flow is found which is 90° out of phase with the pressure gradient (right graph of Fig. 9). The flow is dominated by inertia.

Arbitrary Womersley number flow. Substitution of Eq. (2.6) and (2.7) in Eq. (2.2) yields:

$$\nu\frac{\partial^2 \hat{v}_z(r)}{\partial r^2} + \frac{\nu}{r}\frac{\partial \hat{v}_z(r)}{\partial r} - i\omega\hat{v}_z(r) = \frac{1}{\rho}\frac{\partial \hat{p}}{\partial z}. \tag{2.14}$$

Substitution of

$$s = i^{3/2}\alpha r/a \tag{2.15}$$

in the homogeneous part of this equation yields the equation of Bessel for $n = 0$:

$$\frac{\partial^2 \hat{v}_z}{\partial s^2} + \frac{1}{s}\frac{\partial \hat{v}_z}{\partial s} + \left(1 - \frac{n^2}{s^2}\right)\hat{v}_z = 0 \tag{2.16}$$

with solution given by the Bessel functions of the first kind:

$$J_n(s) = \sum_{k=0}^{\infty}\frac{(-1)^k}{k!(n+k)!}\left(\frac{s}{2}\right)^{2k+n} \tag{2.17}$$

so:

$$J_0(s) = \sum_{k=0}^{\infty}\frac{(-1)^k}{k!k!}\left(\frac{s}{2}\right)^{2k} = 1 - \left(\frac{s}{2}\right)^2 + \frac{1}{1^2 2^2}\left(\frac{z}{2}\right)^4 - \frac{1}{1^2 2^2 3^2}\left(\frac{z}{2}\right)^6 + \ldots \tag{2.18}$$

see also [1]. Together with the particular solution:

$$\hat{v}_z^p = \frac{i}{\rho\omega}\frac{\partial \hat{p}}{\partial z} \tag{2.19}$$

we have:

$$\hat{v}_z(s) = KJ_0(s) + \hat{v}_z^p. \tag{2.20}$$

Using the boundary condition $\hat{v}_z(a) = 0$ then yields:

$$K = -\frac{\hat{v}_z^p}{J_0(\alpha i^{3/2})} \tag{2.21}$$

and finally:

$$\hat{v}_z(r) = \frac{i}{\rho\omega}\frac{\partial \hat{p}}{\partial z}\left[1 - \frac{J_0(i^{3/2}\alpha r/a)}{J_0(i^{3/2}\alpha)}\right]. \tag{2.22}$$

These are the well known Womersley profiles, [8] displayed in Fig. 10. As can be seen from this figure, the Womersley profiles for intermediate

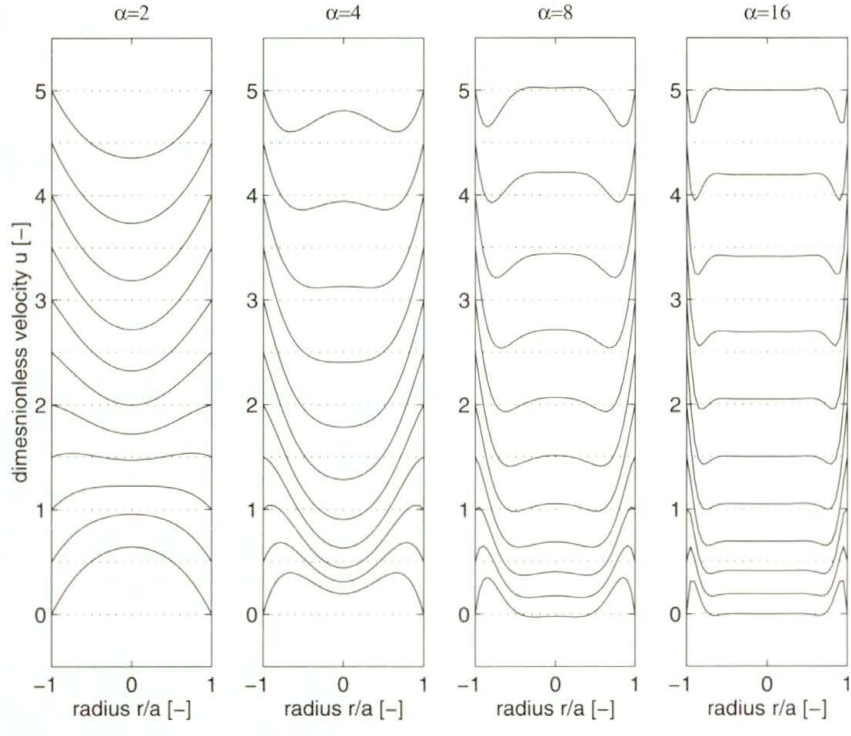

FIGURE 10. Womersley profiles for different Womersley numbers ($\alpha = 2, 4, 8, 16$)

Womersley numbers are characterized by a phase-shift between the flow in the boundary layer and the flow in the central core of the tube. Actually, in the boundary layer viscous forces dominate the inertia forces and the flow behaves like the flow for small Womersley numbers. For high enough Womersley numbers, in the central core, inertia forces are dominant and flattened profiles that are shifted in phase are found. The thickness of the non-stationary boundary layer is determined by the Womersley number. This will be discussed in more detail in Sec. 2.1.2.

Wall shear stress

Using the property of Bessel functions, see [1]

$$\frac{\partial J_0(s)}{\partial s} = -J_1(s) \tag{2.23}$$

and the definition of the Womersley function

$$F_{10}(\alpha) = \frac{2J_1(i^{3/2}\alpha)}{i^{3/2}\alpha J_0(i^{3/2}\alpha)} \tag{2.24}$$

the wall shear stress defined as:

$$\tau_w = -\eta \left.\frac{\partial v_z}{\partial r}\right|_{r=a} \tag{2.25}$$

can be derived as:

$$\tau_w = -\frac{a}{2} F_{10}(\alpha) \frac{\partial p}{\partial z} = F_{10}(\alpha)\tau_w^p \tag{2.26}$$

with τ_w^p the wall shear stress for Poiseuille flow. In Fig. 11 the function $F_{10}(\alpha)$ and thus a dimensionless wall shear stress τ_w/τ_w^p is given as a function of α.

Remark 1.

$$J_1(s) = \sum_{k=0}^{\infty} \frac{(-1)^k}{k!(1+k)!} \left(\frac{s}{2}\right)^{2k+1} = \left(\frac{s}{2}\right) - \frac{1}{1^2 2} \left(\frac{z}{2}\right)^3 + \frac{1}{1^2 2^2 3} \left(\frac{z}{2}\right)^5 + \dots \tag{2.27}$$

In many cases, for instance to investigate limiting values for small and large values of α, it is convenient to approximate the Womersley function with:

$$F_{10}(\alpha) \approx \frac{(1+\beta)^{1/2}}{(1+\beta)^{1/2} + 2\beta} \qquad \text{with} \qquad \beta = \frac{i\alpha^2}{16}. \tag{2.28}$$

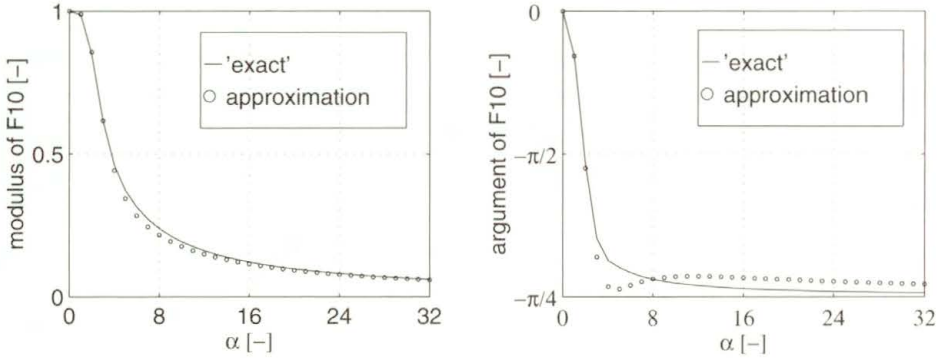

FIGURE 11. Modulus (left) and argument (right) of the function $F_{10}(\alpha)$ or τ_w/τ_w^p as a function of α. The approximations are indicated with dotted and dashed lines.

This approximation is plotted with dotted lines in Fig. 11. For small values of the Womersley number ($\alpha < 3$) the following approximation derived from Eq. (2.28) can be used:

$$F_{10}(\alpha) \approx \frac{1}{1+2\beta} = \frac{1}{1+i\alpha^2/8} \tag{2.29}$$

whereas for large values ($\alpha > 15$) one may use:

$$F_{10}(\alpha) \approx \frac{1}{2}\beta^{-1/2} = \frac{(1-i)\sqrt{2}}{\alpha}. \tag{2.30}$$

These two approximations are plotted with dashed lines in Fig. 11. Note that the dimensionless wall shear stress for large values of α approximates zero and not ∞ that one could conclude from the steep gradients in the velocity profiles in Fig. 10.

The mean flow q can be derived using the property, see [1]:

$$s\frac{\partial J_n(s)}{\partial s} = -nJ_n(s) + sJ_{n-1}(s). \tag{2.31}$$

For $n = 1$ it follows that:

$$sJ_0(s)ds = d(sJ_1(s)) \tag{2.32}$$

and together with $J_1(0) = 0$ the flow becomes:

$$q = \int_0^a \hat{v}_z 2\pi r dr = i\frac{\pi a^2}{\rho\omega}\left[1 - F_{10}(\alpha)\right]\frac{\partial p}{\partial z} = \left[1 - F_{10}(\alpha)\right]\hat{q}_\infty$$

$$= \frac{8i}{\alpha^2}\left[1 - F_{10}(\alpha)\right]\hat{q}_p \quad (2.33)$$

with

$$\hat{q}_\infty = \frac{i\pi a^2}{\rho\omega}\frac{\partial \hat{p}}{\partial z} \qquad \text{and} \qquad \hat{q}_p = \frac{\pi a^4}{8\eta}\frac{\partial \hat{p}}{\partial z}. \quad (2.34)$$

Combining Eq. (2.26) with Eq. (2.33) by elimination of $\partial p/\partial z$ finally yields:

$$\tau_w = \frac{a}{2A} i\omega\rho \frac{F_{10}(\alpha)}{1 - F_{10}(\alpha)} q. \quad (2.35)$$

With $A = \pi a^2$ the cross-sectional area of the tube. In the next section this expression for the wall shear stress will be used to approximate the shear forces that the fluid exerts on the wall of the vessel.

Vascular impedance

The longitudinal impedance defined as:

$$Z_L = -\frac{\partial p}{\partial z}\frac{1}{q} \quad (2.36)$$

can be derived directly from Eq. (2.33) and reads:

$$Z_L = i\omega\frac{\rho}{\pi a^2}\frac{1}{1 - F_{10}(\alpha)}. \quad (2.37)$$

For a Poiseuille profile the longitudinal impedance is defined by integration of Eq. (2.10) and is given by:

$$Z_p = \frac{8\eta}{\pi a^4}. \quad (2.38)$$

From this it can be derived that the impedance of a rigid tube for oscillating flow related to the impedance for steady flow (Poiseuille resistance) is given by the following equation:

$$\frac{Z_L}{Z_p} = \frac{i\alpha^2}{8}\frac{1}{1 - F_{10}(\alpha)}. \quad (2.39)$$

In Fig. 12 the relative impedance is plotted as a function of the Womersley number α. The relative longitudinal impedance is real for $\alpha \ll 1$ and becomes imaginary for $\alpha \to \infty$. This expresses the fact that for low frequencies (or small diameters) the viscous forces are dominant, whereas for high frequencies (or large diameters) inertia is dominant and the flow behaves as an inviscid flow.

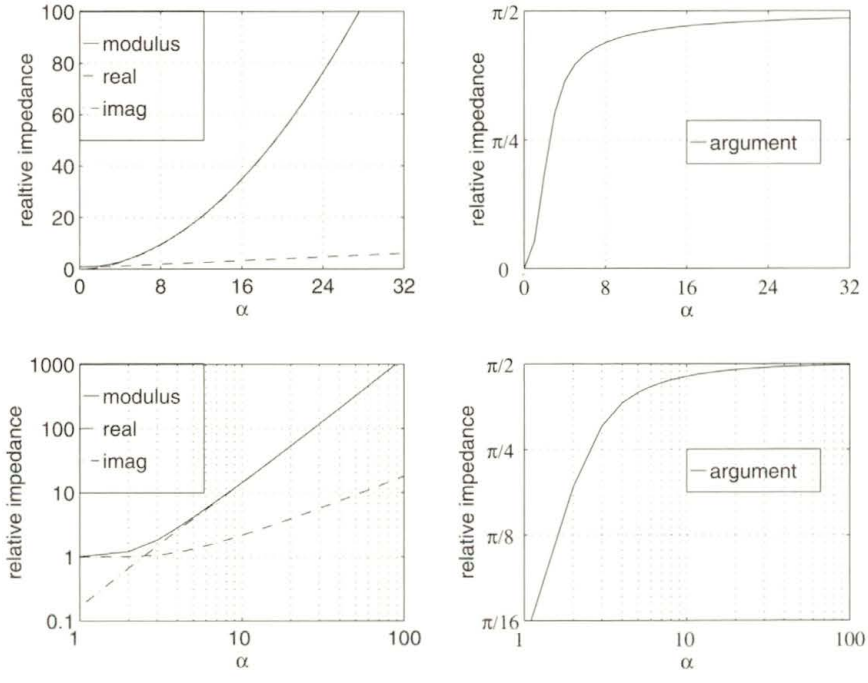

FIGURE 12. The relative impedance for oscillating flow in a tube (linear scale at the top and logarithmic scale at the bottom) as a function of α.

For small values of α the relative impedance results in (see 2.29):

$$\frac{Z_L(\alpha < 3)}{Z_p} \approx 1 + \frac{i\alpha^2}{8}. \tag{2.40}$$

Viscous forces then dominate and the pressure gradient is in phase with the flow and does not (strongly) depend on alpha. For large values of α Eq. (2.30) gives:

$$\frac{Z_L(\alpha > 15)}{Z_p} \approx \frac{i\alpha^2}{8} \tag{2.41}$$

indicating that the pressure gradient is out of phase with the flow and increases quadratically with α.

2.1.2. Entrance flow. In general the flow in blood vessels is not fully developed. Due to transitions and bifurcations the velocity profile has to develop from a certain profile at the entrance of the tube (see Fig. 13).

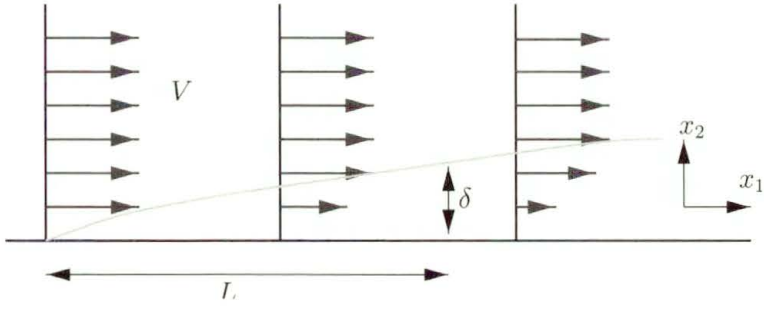

FIGURE 13. Development of a boundary layer

In order to obtain an idea of the length needed for the flow to develop, the flow with a characteristic velocity V along a smooth boundary with characteristic length L is considered. Viscous forces only play an important role in the small boundary layer with thickness δ. Outside the boundary layer the flow is assumed to be inviscid so that Bernoulli's law can be applied. From this configuration simplified Navier-Stokes equations can be derived by assuming that $\delta \ll L$ and the order of magnitude of its terms can be estimated:

$$\begin{cases} \dfrac{\partial v_1}{\partial x_1} + \dfrac{\partial v_2}{\partial x_2} = 0, \\ O\left(\dfrac{V}{L}\right) \quad O\left(\dfrac{v}{\delta}\right), \\ \rho\dfrac{\partial v_1}{\partial t} + \rho v_1\dfrac{\partial v_1}{\partial x_1} + \rho v_2\dfrac{\partial v_1}{\partial x_2} = -\dfrac{\partial p}{\partial x_1} + \eta\dfrac{\partial^2 v_1}{\partial {x_1}^2} + \eta\dfrac{\partial^2 v_1}{\partial {x_2}^2}, \\ O(\omega V) \quad O\left(\dfrac{V^2}{L}\right) \quad O\left(\dfrac{V^2}{L}\right) \quad O\left(\dfrac{1}{\rho}\dfrac{\partial p}{\partial x}\right) \quad O\left(\dfrac{\nu V}{L^2}\right) \quad O\left(\nu V/\delta^2\right). \end{cases} \tag{2.42}$$

This shows clearly that the diffusive forces are determined by second order derivatives of the velocity normal to the boundary. Moreover it can be seen that the stationary inertia forces are of the same order of magnitude as the viscous forces (which is the case at the boundary layer $x_2 = \delta$) as long as:

$$O\left(\frac{\nu V}{\delta^2}\right) = O\left(\frac{V^2}{L}\right). \tag{2.43}$$

Steady flow

If the entrance length of the flow in a tube is defined as the length needed for the boundary layer to contain the complete cross section, i.e. $\delta = a$, then the ratio of the entrance length and the radius of the tube follows from the equation above as:

$$\frac{L_e}{a} = O\left(\frac{aV}{\nu}\right), \tag{2.44}$$

or with the definition of the Reynolds number $\mathrm{Re} = 2aV/\nu$ the dimensionless entrance length $L_e/2a$ is found to be proportional to the Reynolds number:

$$\frac{L_e}{2a} = O(\mathrm{Re}). \tag{2.45}$$

In [6] one can find that for laminar flow, for $L_e : v(L_e, 0) = 0.99 \cdot 2V$:

$$\frac{L_e}{2a} = 0.056\mathrm{Re}. \tag{2.46}$$

For steady flow in the carotid artery, for instance, $\mathrm{Re} = 300$, and thus $L_e \approx 40a$. This means that the flow will never become fully developed since the length of the carotid artery is much less than 40 times its radius. In arterioles and smaller vessels, however, $\mathrm{Re} < 10$ and hereby $L_e < a$, so fully developed flow will be found in many cases.

Oscillating flow

For oscillating flow the inlet length is smaller as compared to the inlet length for steady flow. This can be seen from the following. The unsteady inertia forces are of the same magnitude as the viscous forces when:

$$O(V\omega) = O\left(\frac{\nu V}{\delta^2}\right) \tag{2.47}$$

and thus:

$$\delta = O\left(\sqrt{\frac{\nu}{\omega}}\right). \tag{2.48}$$

This means that for fully developed oscillating flow a boundary layer exists with a relative thickness of:

$$\frac{\delta}{a} = O\left(\alpha^{-1}\right). \tag{2.49}$$

If, for oscillating flow, the inlet length is defined as the length for which the viscous forces still are of the same magnitude as the stationary inertia forces, i.e.:

$$O\left(\frac{\nu V}{\delta^2}\right) = O\left(\frac{V^2}{L_e}\right) \tag{2.50}$$

then together with Eq. (2.49) the inlet length is of the order

$$L_e = O\left(\frac{V\delta^2}{\nu}\right) = O\left(\frac{a}{\alpha^2}\,\mathrm{Re}\right). \tag{2.51}$$

Note that this holds only for $\alpha > 1$. For $\alpha < 1$ the boundary layer thickness is restricted to the radius of the tube and we obtain an inlet length of the same magnitude as for steady flow.

2.2. Steady and Pulsating Flow in Curved and Branched Tubes

2.2.1. Steady flow in a curved tube

Steady entrance flow in a curved tube

The flow in a curved tube is determined by an equilibrium of convective forces, pressure forces and viscous forces. Consider, the entrance flow in a curved tube with radius a and a radius of curvature R_0. With respect to the origin O we can define a cylindrical coordinate system (R, z, ϕ). At the entrance (A: $R_0 - a < R < R_0 + a$, $-a < z < a$, $\phi = 0$) a uniformly distributed irotational (plug) flow $v_\phi = V$ (see Fig. 14) is assumed. As long as the boundary layer has not yet developed ($R_0\phi \ll 0.1a\,\mathrm{Re}$) the viscous forces are restricted to a very thin boundary layer and the velocity is restricted to one component, v_ϕ. The other components (v_R and v_z) are small compared to v_ϕ. In the core the flow is inviscid so Bernoulli's law can be applied:

$$p + \tfrac{1}{2}\rho v_\phi^2 = \text{constant}. \tag{2.52}$$

With p the pressure, and ρ the density of the fluid. The momentum equation in R-direction shows an equilibrium of pressure forces and centrifugal forces:

$$\frac{\partial p}{\partial R} = \frac{\rho v_\phi^2}{R}. \tag{2.53}$$

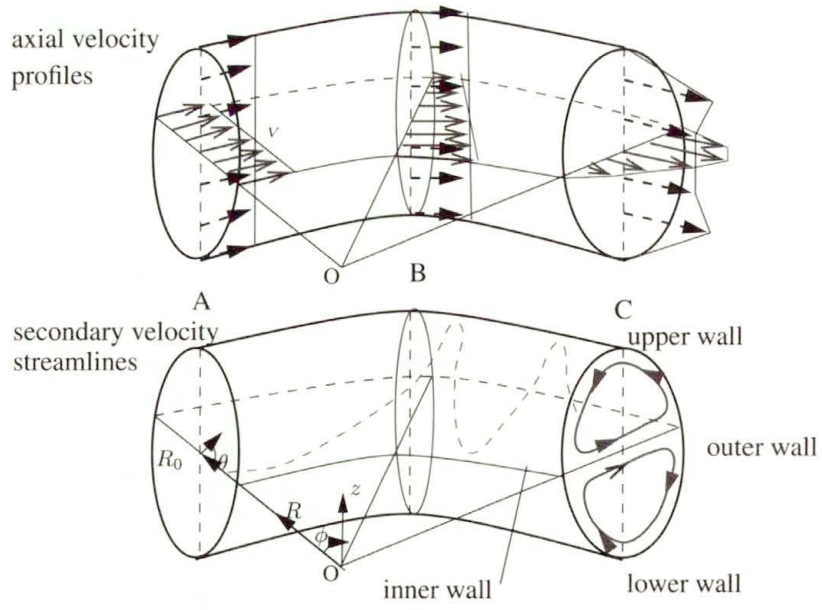

FIGURE 14. Axial velocity profiles, secondary velocity streamlines and helical motion of particles for entrance flow in a curved tube.

As a consequence, the pressure is largest at the outer wall and smallest at the inner wall. Together with Bernoulli's law it follows that the velocity will become largest at the inner wall and lowest at the outer wall of the tube (see Fig. 14 location (B)). Indeed, elimination of the pressure from Eq. (2.52) and Eq. (2.53) yields:

$$\frac{\partial v_\phi}{\partial R} = -\frac{v_\phi}{R} \tag{2.54}$$

and thus:

$$v_\phi = \frac{k_1}{R}. \tag{2.55}$$

The constant k_1 can be determined from the conservation of mass in the plane of symmetry ($z = 0$):

$$2aV = \int_{R_0-a}^{R_0+a} v_\phi(R')dR' = k_1 \ln \frac{R_0 + a}{R_0 - a} \tag{2.56}$$

and thus:

$$k_1 = \frac{2aV}{\ln \frac{1+\delta}{1-\delta}} \tag{2.57}$$

with $\delta = a/R_0$. So in the entrance region ($\phi \ll 0.1\delta\,\mathrm{Re}$) initially the following velocity profile will develop:

$$v_\phi(R) = \frac{2aV}{R \ln \frac{1+\delta}{1-\delta}}. \tag{2.58}$$

It is easy to derive that for small values of δ this reduces to $v_\phi(R) = (R_0/R)V$.

Note that the velocity profile does only depend on R and does not depend on the azimuthal position θ in the tube. In terms of the toroidal coordinate system (r, θ, ϕ) we have:

$$R(r, \theta) = R_0 - r\cos\theta \tag{2.59}$$

and the velocity profile given in Eq. (2.58) is:

$$v_\phi(r, \theta) = \frac{2aV}{(R_0 - r\cos\theta) \ln \frac{1+\delta}{1-\delta}} = \frac{2\delta V}{(1 - \delta(r/a)\cos\theta) \ln \frac{1+\delta}{1-\delta}}. \tag{2.60}$$

Again for small values of δ this reduces to

$$v_\phi(r, \theta) = \frac{V}{1 - \delta(r/a)\cos\theta}.$$

Going more downstream, due to viscous forces a boundary layer will develop along the walls of the tube and will influence the complete velocity distribution. Finally the velocity profile will look like the one that is sketched at position C. This profile does depend on the azimuthal position. In the plane of symmetry it will have a maximum that is shifted to the outer wall. In the direction perpendicular to the plane of symmetry an M-shaped profile will be found (see Fig. 14). This velocity distribution can only be explained if we also consider the secondary flow field, i.e. the velocity components in the plane of a cross-section ($\phi = \text{const.}$) of the tube perpendicular to the axis.

Viscous forces will diminish the axial velocity in the boundary layer along the wall of the curved tube. As a result, the equilibrium between the pressure gradient in R-direction and the centrifugal forces will be disturbed. In the boundary layers we will have $\rho V^2/R < \partial p/\partial R$ and in the central core $\rho V^2/R > \partial p/\partial R$. Consequently the fluid particles in the central core will accelerate towards the outer wall, whereas fluid particles in the boundary layer will accelerate in opposite direction. In this way a secondary vortex will develop as indicated in Fig. 14. This motion of fluid particles from the inner wall towards the outer wall in the core and along the upper and lower

walls back to the inner wall will have consequences for the axial velocity distribution. Particles with a relatively large axial velocity will move to the outer wall and due to convective forces, the maximum of the axial velocity will shift in the same direction. On the other hand, particles in the boundary layer at the upper and lower walls will be transported towards the inner wall and will convect a relatively low axial velocity. In this way in the plane of symmetry an axial velocity profile will develop with a maximum at the outer wall, and a minimum at the inner wall. For large curvatures or large Reynolds numbers even negative axial velocity at the inner wall can occur due to boundary layer separation.

Once the maximum of the axial velocity is located near the outer wall, the secondary flow will transport particles with a relatively large axial velocity along the upper and lower walls and a C-shaped axial velocity contour will develop. This can clearly be seen in Fig. 15 where for different curvatures of the tube contour plots of the axial velocity and streamlines of the secondary velocity are given. Note that the combination of the axial and secondary flow results in a helical movement of the fluid particles (see Fig. 14). While moving in downstream direction the particles move from the inner wall towards the outer wall and back to the inner wall along the upper (or lower) wall.

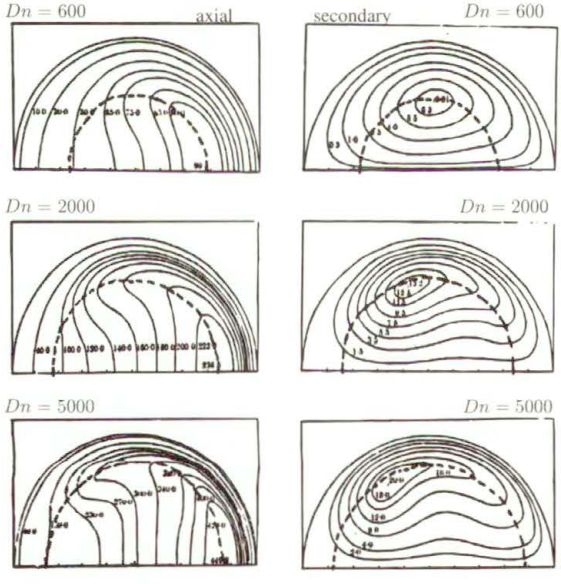

FIGURE 15. Contour plots of axial (left) and streamline plots of secondary (right) fully developed steady flow in a curved tube for Dean numbers of 600 (top), 2000 (middle) and 5000 (bottom) as computed by Collins and Dennis in [2].

Steady fully developed flow in a curved tube

In order to obtain a more quantitative description of the flow phenomena it is convenient to use the toroidal coordinate system (r, θ, ϕ) as is depicted in Fig. 14. The corresponding velocity components are v_r, v_θ and v_ϕ. The Navier-Stokes equations in toroidal coordinates read [7]:

- in r-direction:

$$\frac{\partial v_r}{\partial t} + \frac{1}{rB}\left[\frac{\partial}{\partial r}(rBv_r^2) + \frac{\partial}{\partial \theta}(Bv_r v_\theta) + \frac{\partial}{\partial \phi}(\delta r v_\phi v_r) - Bv_\theta^2 - \delta r \cos\theta v_\phi^2\right]$$

$$= -\frac{\partial p}{\partial r} + \frac{1}{\mathrm{Re}}\left\{\frac{1}{rB}\left[\frac{\partial}{\partial r}\left(rB\frac{\partial v_r}{\partial r}\right) + \frac{\partial}{\partial \theta}\left(\frac{B}{r}\frac{\partial v_r}{\partial \theta}\right) + \frac{\partial}{\partial \phi}\left(\frac{\delta^2 r}{B}\frac{\partial v_r}{\partial \phi}\right)\right]\right.$$

$$\left. - \frac{1}{r^2}\left(2\frac{\partial v_\theta}{\partial \theta} + v_r\right) + \frac{\delta \sin\theta v_\theta}{rB} + \frac{\delta^2 \cos\theta}{B^2}\left(v_\theta \sin\theta - v_r \cos\theta - 2\frac{\partial v_\phi}{\partial \phi}\right)\right\}, \tag{2.61}$$

- in θ-direction:

$$\frac{\partial v_\theta}{\partial t} + \frac{1}{rB}\left[\frac{\partial}{\partial r}(rBv_r v_\theta) + \frac{\partial}{\partial \theta}(Bv_\theta^2) + \frac{\partial}{\partial \phi}(\delta r v_\phi v_\theta) + Bv_r v_\theta + \delta r \sin\theta v_\phi^2\right]$$

$$= -\frac{\partial p}{\partial \theta} + \frac{1}{\mathrm{Re}}\left\{\frac{1}{rB}\left[\frac{\partial}{\partial r}\left(rB\frac{\partial v_\theta}{\partial r}\right) + \frac{\partial}{\partial \theta}\left(\frac{B}{r}\frac{\partial v_\theta}{\partial \theta}\right) + \frac{\partial}{\partial \phi}\left(\frac{\delta^2 r}{B}\frac{\partial v_\theta}{\partial \phi}\right)\right]\right.$$

$$\left. + \frac{1}{r^2}\left(2\frac{\partial v_r}{\partial \theta} - v_\theta\right) - \frac{\delta \sin\theta v_r}{rB} - \frac{\delta^2 \sin\theta}{B^2}\left(v_\theta \sin\theta - v_r \cos\theta - 2\frac{\partial v_\phi}{\partial \phi}\right)\right\}, \tag{2.62}$$

- in ϕ-direction:

$$\frac{\partial v_\phi}{\partial t} + \frac{1}{rB}\left[\frac{\partial}{\partial r}(rBv_\phi v_r) + \frac{\partial}{\partial \theta}(Bv_\phi v_\theta) + \frac{\partial}{\partial \phi}(\delta r v_\phi^2)\right.$$

$$\left. + \delta r v_\phi (v_r \cos\theta - v_\theta \sin\theta)\right] = -\frac{\delta}{B}\frac{\partial p}{\partial \phi}$$

$$+ \frac{1}{\mathrm{Re}}\left\{\frac{1}{rB}\left[\frac{\partial}{\partial r}\left(rB\frac{\partial v_\phi}{\partial r}\right) + \frac{\partial}{\partial \theta}\left(\frac{B}{r}\frac{\partial v_\phi}{\partial \theta}\right) + \frac{\partial}{\partial \phi}\left(\frac{\delta^2 r}{B}\frac{\partial v_\phi}{\partial \phi}\right)\right]\right.$$

$$\left. + \frac{2\delta^2}{B^2}\left(\frac{\partial v_r}{\partial \phi}\cos\theta - \frac{\partial v_\theta}{\partial \phi}\sin\theta - \frac{v_\phi}{2}\right)\right\}, \tag{2.63}$$

continuity:

$$\frac{\partial}{\partial r}(rBv_r) + \frac{\partial}{\partial \theta}(Bv_\theta) + \frac{\partial}{\partial \phi}(\delta r v_\phi) = 0 \tag{2.64}$$

with

$$\delta = \frac{a}{R_0} \qquad \text{and} \qquad B = 1 + \delta r \cos\theta.$$

For fully developed flow all derivatives in ϕ direction are zero ($\partial/\partial\phi = 0$). This of course does not hold for the driving force $\partial p/\partial\phi$. If we scale according to:

$$r^* = \frac{r}{a}, \quad p^* = \frac{p}{\rho V^2}, \quad v_r^* = \frac{v_r}{V}, \quad v_\theta^* = \frac{v_\theta}{V}, \quad v_\phi^* = \frac{v_\phi}{V} \tag{2.65}$$

the continuity equation and the momentum equation in r-direction read, after dropping the asterisk:

$$\frac{\partial v_r}{\partial r} + \frac{v_r}{r}\left[\frac{1 + 2\delta r\cos\theta}{1 + \delta r\cos\theta}\right] + \frac{1}{r}\frac{\partial v_\theta}{\partial \theta} - \frac{\delta v_\theta \sin\theta}{1 + \delta r\cos\theta} = 0 \tag{2.66}$$

and

$$v_r\frac{\partial v_r}{\partial r} + \frac{v_\theta}{r}\frac{\partial v_r}{\partial \theta} - \frac{v_\theta^2}{r} - \delta\frac{v_\phi^2\cos\theta}{1 + \delta r\cos\theta}$$

$$= -\frac{\partial p}{\partial r} + \frac{1}{\mathrm{Re}}\left[\left(\frac{1}{r}\frac{\partial}{\partial\theta} - \frac{\delta\sin\theta}{1 + \delta r\cos\theta}\right)\left(\frac{1}{r}\frac{\partial v_r}{\partial\theta} - \frac{\partial v_\theta}{\partial r} - \frac{v_\theta}{r}\right)\right]. \tag{2.67}$$

The two important dimensionless parameters that appear are the curvature ratio δ and the Reynolds number Re defined as:

$$\delta = \frac{a}{R_0} \qquad \text{and} \qquad Re = \frac{2aV}{\nu} \tag{2.68}$$

with a the radius and R_0 the curvature of the tube. If we restrict ourselves to the plane of symmetry ($\theta = 0, \pi$, $\cos\theta = \pm 1$ and $v_\theta = 0$) we have for the momentum equation:

$$v_r\frac{\partial v_r}{\partial r} - \delta\frac{\pm v_\phi^2}{1 \pm \delta r} = -\frac{\partial p}{\partial r} + \frac{1}{\mathrm{Re}}\left[\left(\frac{1}{r}\frac{\partial}{\partial\theta}\right)\left(\frac{1}{r}\frac{\partial v_r}{\partial\theta} - \frac{\partial v_\theta}{\partial r}\right)\right]. \tag{2.69}$$

If we consider small curvatures ($\delta \ll 1$) only, knowing that $v_\phi = O(1)$ and r is already scaled and in the interval $[0, 1]$, the momentum equation yields

$$v_r\frac{\partial v_r}{\partial r} = O(\delta v_\phi^2) = O(\delta)$$

and thus $O(v_r) = \delta^{1/2}$. From the continuity equation Eq. (2.66) it can be seen that v_r and v_θ scale in the same way, i.e. $O(v_r) = O(v_\theta)$, and thus also $O(v_\theta) = \delta^{1/2}$. If instead of using Eq. (2.65) we would use:

$$r^* = \frac{r}{a}, \quad p^* = \frac{p}{\delta\rho V^2}, \quad v_r^* = \frac{v_r}{\delta^{1/2}V}, \quad v_\theta^* = \frac{v_\theta}{\delta^{1/2}V}, \quad v_\phi^* = \frac{v_\phi}{V} \tag{2.70}$$

the continuity equation and momentum equation in r-direction for $\delta \ll 1$ would be (again after dropping the asterisk):

$$\frac{\partial v_r}{\partial r} + \frac{v_r}{r} + \frac{1}{r}\frac{\partial v_\theta}{\partial \theta} = 0 \tag{2.71}$$

and

$$v_r\frac{\partial v_r}{\partial r} + \frac{v_\theta}{r}\frac{\partial v_r}{\partial \theta} - \frac{v_\theta^2}{r} - v_\phi^2\cos\theta = -\frac{\partial p}{\partial r} + \frac{1}{\delta^{1/2}\mathrm{Re}}\left[\frac{1}{r}\frac{\partial}{\partial\theta}\left(\frac{1}{r}\frac{\partial v_r}{\partial\theta} - \frac{\partial v_\theta}{\partial r} - \frac{v_\theta}{r}\right)\right]. \tag{2.72}$$

From this we can see that for small curvature another dimensionless parameter, the Dean number, can be defined as:

$$\mathrm{Dn} = \delta^{1/2}\mathrm{Re}. \tag{2.73}$$

The secondary flow depends on two important parameters, the Reynolds number Re and the curvature δ or the Dean number Dn and the curvature δ. The last combination is often used because for small curvature only the Dean number is of importance.

For large Dean numbers the viscous term in Eq. (2.72) can be neglected in the core of the secondary flow field and one can talk about a boundary layer of the secondary flow. The thickness δ_s of this boundary layer can be derived from the momentum equation in θ-direction:

$$v_r\frac{\partial v_\theta}{\partial r} + \frac{v_\theta}{r}\frac{\partial v_\theta}{\partial\theta} - \frac{v_r v_\theta}{r} + \delta\frac{v_\phi^2\sin\theta}{1+\delta r\cos\theta} = -\frac{1}{r}\frac{\partial p}{\partial\theta} + \frac{1}{\delta^{1/2}\,\mathrm{Re}}\left[\left(\frac{\partial}{\partial r} + \frac{\delta\cos\theta}{1+\delta r\cos\theta}\right)\left(\frac{\partial v_\theta}{\partial r} + \frac{v_\theta}{r} - \frac{1}{r}\frac{\partial v_r}{\partial r}\right)\right]. \tag{2.74}$$

If we assume that at $r = a - \delta_s$ the viscous and inertia forces are of the same order of magnitude we have:

$$\frac{\delta_s}{a} = O(\mathrm{Dn}^{-1/2}). \tag{2.75}$$

In Fig. 15 the boundary layer of the secondary flow is indicated with a dashed line and indeed decreases with increasing Dean numbers.

2.2.2. Unsteady fully developed flow in a curved tube. In unsteady flow in a curved tube the secondary flow will have the same orientation as in stationary flow. The reason for this is that the centrifugal forces are not sensitive for the direction of the axial velocity ($f_c \propto v_\phi^2$). For high frequencies, or better large Womersley numbers, like in the case for straight tubes an nonstationary boundary layer will develop such that in the central core the flow will behave more or less inviscid whereas at the boundary viscous forces are dominant. For oscillatory flow this may lead to a secondary flow field as is depicted in Fig. 16. In the core the secondary vortex will have an opposite direction as in the boundary layer where the direction corresponds with the one in steady flow. In contradiction to the flow in a straight tube, however, for flow in a curved tube the superposition of several harmonics is not allowed because the governing equations are strongly non-linear.

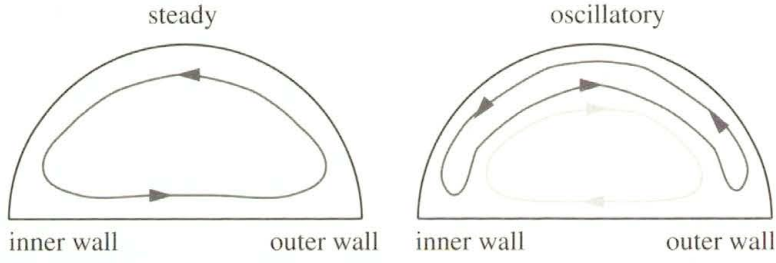

FIGURE 16. Streamline patterns of fully developed secondary flow in steady (left) and oscillatory (right) flow in a curved tube.

In pulsating flow this second vortex will not be that pronounced as in oscillating flow but some influence can be depicted. This is shown in the Fig. 17 where the results of a finite element computation of pulsating flow in a curved tube are given together with experimental (laser Doppler) data.

2.2.3. Flow in branched tubes. The flow in branched tubes (bifurcations) shows the same phenomena as in curved tubes. Actually the bifurcation can be considered as a two joined curved tubes. Of course there are also differences with curved tube flow due to the bifurcation point (apex) which will induce an extra asymmetry (see Fig. 18).

Detailed knowledge about the flow phenomena in curved and branched tubes is of great physiological and clinical importance. The prediction of areas of high and low shear rates and wall shear stress, the prediction of

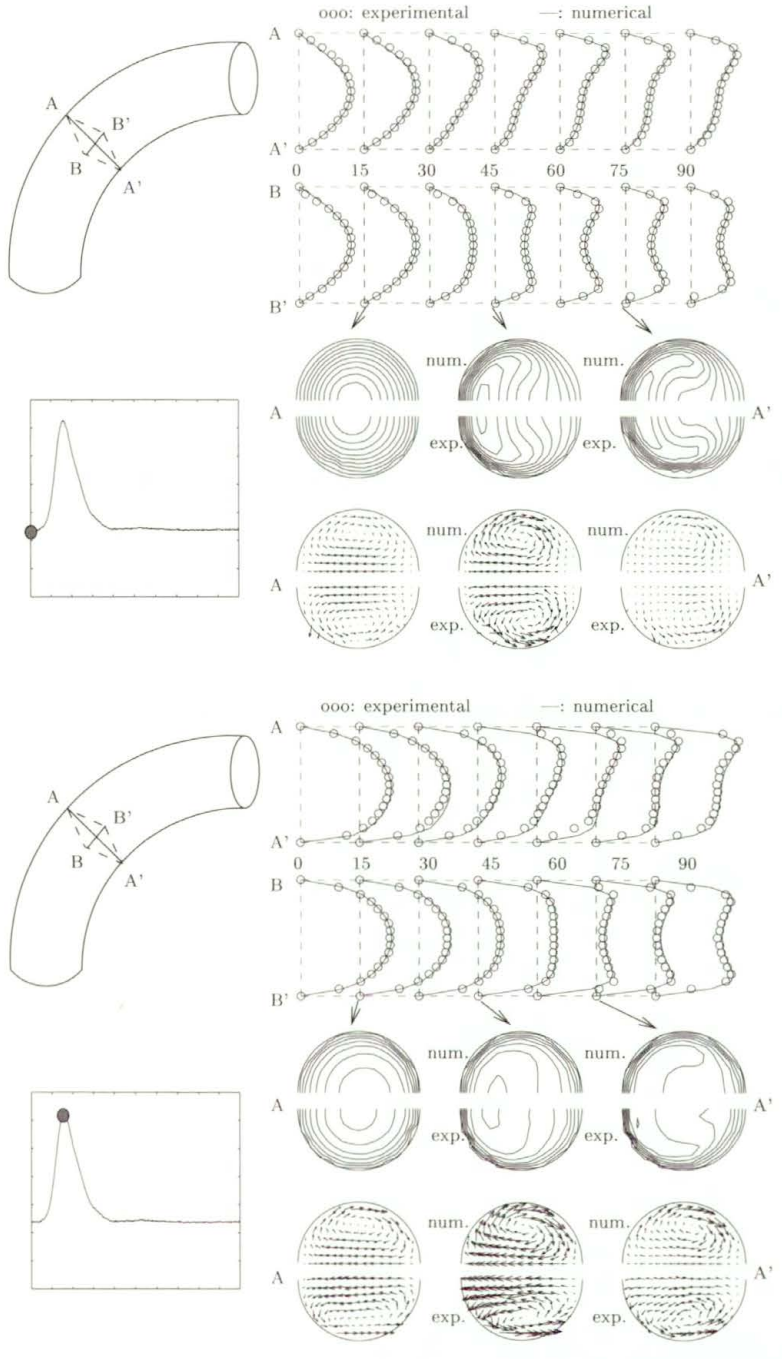

FIGURE 17. Computational (FEM) and experimental (LDA) results of pulsatile flow in a curved tube: end diastolic (top), peak systolic (bottom).

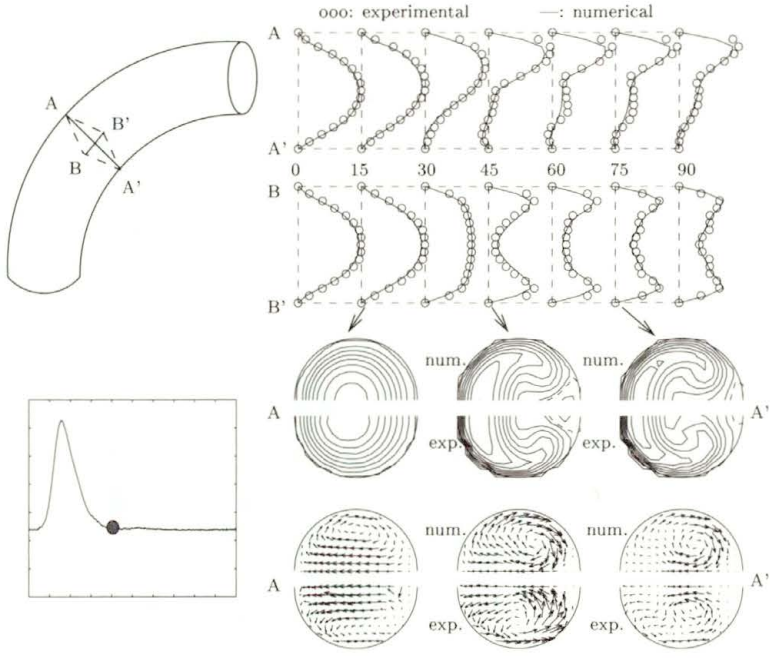

FIGURE 17. Continuation: Computational (FEM) and experimental (LDA) results of pulsatile flow in a curved tube: end systolic.

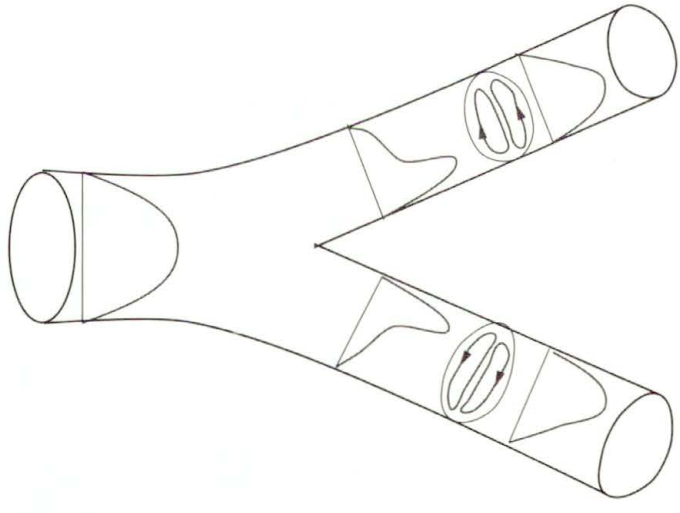

FIGURE 18. Axial velocity and streamline patterns of flow in a bifurcation.

flow instabilities related to high shear rates as occur at the interface between the areas with high and low axial velocity can help to interpret clinical data from ultra-sound Doppler measurements and MRI images and can help to get insight in the development of atherosclerosis. In many case advanced methods in computational fluid dynamics (CFD) are needed to obtain more then the qualitative information as is given in this section. An example of this is given in Fig. 19 where the results of computations of the flow in the internal carotid artery is given together with experimental results obtained with laser Doppler anemometry.

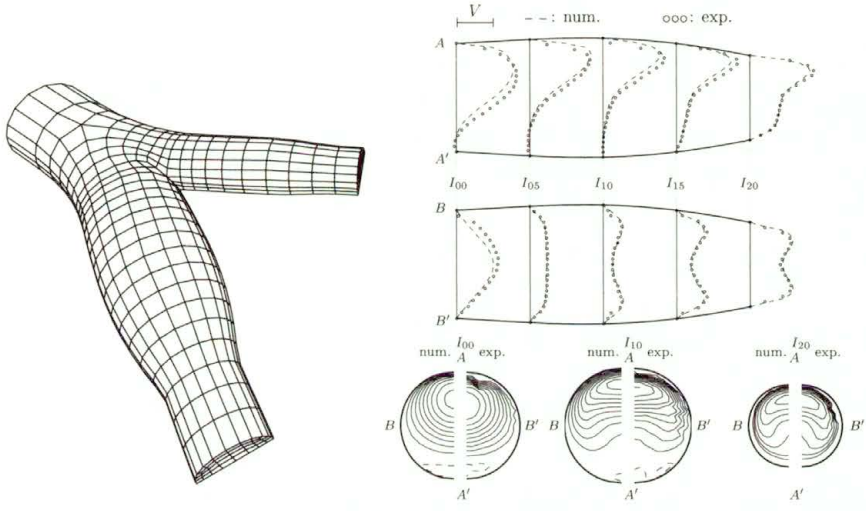

FIGURE 19. Computational (FEM) and experimental (LDA) velocity distributions of a steady flow in a model of the carotid artery bifurcation.

3. Wave Phenomena in Blood Vessels

3.1. Introduction

In this section we will show that traveling pressure and flow waves are the result of the distensibility (or compliance) of the arteries and the pulsatile character of the pressure. A typical relation between the pressure and cross-sectional area of an artery is given in Fig. 5 and shows that the compliance normally does not have a constant value but strongly depends on the pressure. In this section, however, only small area variations will be considered and a linear relation between the pressure amplitude and the vessel diameter

will be assumed. Apart from wave propagation and the importance of viscous forces expressed in the value of the Womersley number α, also wave reflection from arterial bifurcations or transitions in mechanical or geometrical properties will be dealt with. Moreover, attenuation of waves as a result of fluid viscosity and wall visco-elasticity will be discussed.

3.2. Pressure and Flow

In the physiological introduction of this course (Sec. 2) it is mentioned that the heart is a four-chambered pump that generates a pulsating pressure and flow (see Fig. 2). The frequency contents of the pressure and flow in the aorta is given in Table 1 and shows that the pulsatile character of the pressure and flow can be described very well with the first 8 to 10 harmonics (see also Fig. 6). Moreover, in Sec. 2 a simple (windkessel) model was introduced to describe the pressure/flow relation or impedance of the arterial system using the compliance $C_e = dV/dp$ of the elastic arteries and the resistance R_p of the periferal arteries (see also equation 1.9):

$$q_a = C_e \frac{\partial p_a}{\partial t} + \frac{p_a}{R_p} \tag{3.1}$$

and with $p_a = \hat{p}_a e^{i\omega t}$, $q_a = \hat{q}_a e^{i\omega t}$:

$$Z = \frac{p_a}{q_a} = \frac{R_p(1 - i\omega R_p C_e)}{1 + \omega^2 R_p^2 C_e^2}. \tag{3.2}$$

In Fig. 20 the absolute value and argument of the impedance given by Eq. (3.2) is shown as a function of the harmonics. Experimental data (indicated with lines [4]) show that the windkessel model does not predict accurate results especially for the phase of the higher harmonics. Moreover, as illustrated in Fig. 4, the pressure and flow waves change their shape with increasing distance from the heart. This is a result of traveling waves and never can be described by the windkessel model.

In order to describe the pressure and flow in terms of traveling waves (i.e. $p = p(z,t)$ and $q = q(z,t)$) the following complex notation will be used:

$$p(z,t) = \hat{p} e^{i(\omega t - kz)} \qquad \text{and} \qquad q(z,t) = \hat{q} e^{i(\omega t - kz)} \tag{3.3}$$

where ω is the angular frequency, $k = k_r + ik_i$ is the complex wave number and $\hat{p} = |\hat{p}|e^{i\phi}$ denotes the complex amplitude. The actual pressure (c.q. flow)

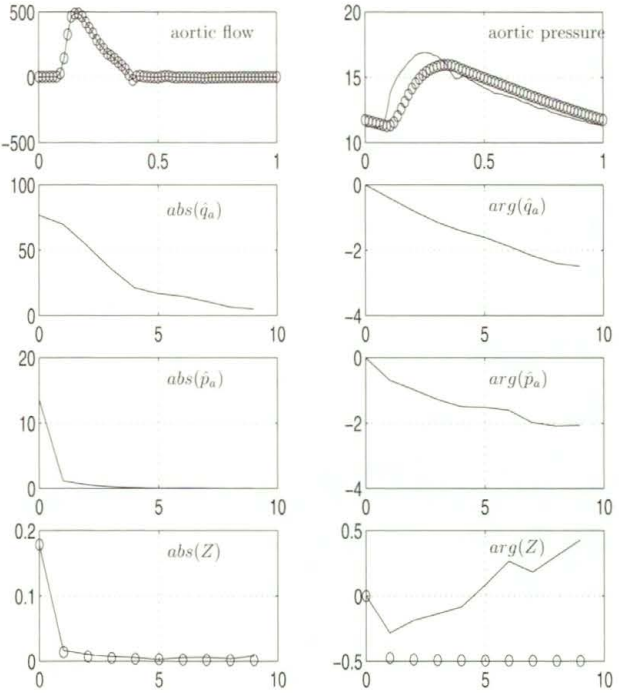

FIGURE 20. Absolute value and argument of the arterial impedance as computed with a windkessel model (o) and from experimental data (–).

is defined as the real part of Eq. (3.3):

$$\mathrm{Re}\,[p(z,t)] = |\hat{p}|e^{k_i z}\cos(\omega t - k_r z + \phi) \tag{3.4}$$

It will be clear that $(-k_i)$ is a measure for the attenuation of the wave and that $k_r = 2\pi/\lambda$ with λ the wavelength.

3.3. Fluid Flow

To analyze fully developed Newtonian flow in distensible tubes we consider the Navier-Stokes equations in a cylindrical coordinate system:

$$\begin{cases} \dfrac{\partial v_r}{\partial t} + v_r\dfrac{\partial v_r}{\partial r} + v_z\dfrac{\partial v_r}{\partial z} = -\dfrac{1}{\rho}\dfrac{\partial p}{\partial r} + \nu\left(\dfrac{\partial}{\partial r}\left(\dfrac{1}{r}\dfrac{\partial}{\partial r}(rv_r)\right) + \dfrac{\partial^2 v_r}{\partial z^2}\right), \\ \dfrac{\partial v_z}{\partial t} + v_r\dfrac{\partial v_z}{\partial r} + v_z\dfrac{\partial v_z}{\partial z} = -\dfrac{1}{\rho}\dfrac{\partial p}{\partial z} + \nu\left(\dfrac{1}{r}\dfrac{\partial}{\partial r}\left(r\dfrac{\partial}{\partial r}(v_z)\right) + \dfrac{\partial^2 v_z}{\partial z^2}\right), \\ \dfrac{1}{r}\dfrac{\partial}{\partial r}(rv_r) + \dfrac{\partial v_z}{\partial z} = 0. \end{cases} \tag{3.5}$$

Since the velocity in circumferential direction equals zero ($v_\phi = 0$), the momentum equation and all derivatives in ϕ-direction are omitted. Due to the distensibility of the tube, pressure and flow waves will propagate with a finite wave speed $c = \omega/k_r$ and a typical wavelength $\lambda = 2\pi/k_r$. First a properly scaled dimensionless form of the Navier-Stokes equations will be derived. To this end the radial coordinates are made dimensionless using the mean radius of the tube, i.e. $r' = r/a_0$. The axial coordinates, however, must be scaled with the real part of the wave number k_r: $z' = zk_r$ (see Eq. (3.3)). The axial velocity is made dimensionless with its characteristic value over a cross-section: $v_z' = v_z/V$. From the continuity equation it can be derived that the radial velocity then must be made dimensionless as: $v_r' = (v_r/V)(1/k_r a)$. The characteristic time $t' = \omega t$ can be written as $t' = (k_r c)t$ with c the wave speed. Together with a dimensionless pressure $p' = p/(\rho V c)$ the dimensionless Navier-Stokes equations read:

$$\begin{cases} \dfrac{\partial v_r'}{\partial t'} + \dfrac{V}{c}\left(v_r'\dfrac{\partial v_r'}{\partial r'} + v_z'\dfrac{\partial v_r'}{\partial z'}\right) \\ \qquad = -\dfrac{1}{k_r^2 a_0^2}\dfrac{\partial p'}{\partial r'} + \dfrac{1}{\alpha^2}\left(\dfrac{\partial}{\partial r'}\left(\dfrac{1}{r'}\dfrac{\partial}{\partial r'}(r'v_r')\right) + a_0^2 k_r^2 \dfrac{\partial^2 v_r'}{\partial z'^2}\right), \\ \dfrac{\partial v_z'}{\partial t'} + \dfrac{V}{c}\left(v_r'\dfrac{\partial v_z'}{\partial r'} + v_z'\dfrac{\partial v_z'}{\partial z'}\right) \\ \qquad = -\dfrac{\partial p'}{\partial z'} + \dfrac{1}{\alpha^2}\left(\dfrac{1}{r'}\dfrac{\partial}{\partial r'}\left(r'\dfrac{\partial}{\partial r'}(v_z')\right) + a_0^2 k_r^2 \dfrac{\partial^2 v_z'}{\partial z'^2}\right), \\ \dfrac{1}{r'}\dfrac{\partial}{\partial r'}(r'v_r') + \dfrac{\partial v_z'}{\partial z'} = 0. \end{cases} \tag{3.6}$$

Besides the Womersley parameter $\alpha = a_0\sqrt{\omega/\nu}$ the dimensionless parameters that play a role in this equation are the speed ratio $S = V/c$ and the circumference-to-wavelength ratio $G = a_0 k_r = 2\pi a_0/\lambda$. Under the assumptions that the wave velocity c is much larger then the fluid velocity V, the wavelength λ is much larger then the tube radius a_0, i.e.:

$$S = \frac{V}{c} \ll 1, \qquad G^2 = (k_r a_0)^2 = \left(\frac{2\pi a_0}{\lambda}\right)^2 \ll 1. \tag{3.7}$$

It can readily be shown that the equations of motion reduce to:

$$\begin{cases} \dfrac{\partial p}{\partial r} = 0, \\ \dfrac{\partial v_z}{\partial t} = -\dfrac{1}{\rho}\dfrac{\partial p}{\partial z} + \nu \dfrac{1}{r}\dfrac{\partial}{\partial r}\left(r\dfrac{\partial v_z}{\partial r}\right), \\ \dfrac{1}{r}\dfrac{\partial}{\partial r}(r v_r) + \dfrac{\partial v_z}{\partial z} = 0. \end{cases} \tag{3.8}$$

If we search for harmonic solutions with angular frequency ω and wave number k:

$$p = \hat{p} e^{i(\omega t - kz)} \tag{3.9}$$

and

$$v_z = \hat{v}_z(r) e^{i(\omega t - kz)} \tag{3.10}$$

substitution in Eq. (3.8) yields exactly the same differential equation for $\hat{v}_z$ as in the case of a rigid tube given in Eq. (2.22). If we further assume that the wall motion is axially restrained, which is thought to be relevant *in vivo* [5], also the boundary condition for $\hat{v}_z$ is not different from the one in rigid tubes but now must be applied in a linearized way at $r = a_0$. It will be clear that in that case we obtain exactly the same Womersley solution given by Eq. (2.22). Substitution of:

$$\frac{\partial \hat{p}}{\partial z} = -ik\hat{p} \tag{3.11}$$

yields:

$$\hat{v}_z(r) = \frac{k}{\rho\omega}\left[1 - \frac{J_0(i^{3/2}\alpha r/a_0)}{J_0(i^{3/2}\alpha)}\right]\hat{p}. \tag{3.12}$$

In [8] a relation similar to Eq. (3.12) is derived, however without the assumption of axial constraint. In that case the second term in the brackets is multiplied by an extra parameter that only slightly differs from unity. The wall shear stress is equal to the wall shear stress for rigid tubes and is defined by Eq. (2.35). The wave number k still has to be determined and depends on the properties of the arterial wall. In the next section the wall motion will be analyzed, again assuming axial restraint.

3.4. Wave Propagation

3.4.1. Derivation of a quasi one-dimensional model. In order to obtain an expression for the wave number introduced in the previous section,

a quasi one-dimensional wave propagation model for pressure and flow waves will be derived. To this end the Leibnitz formulae (or Reynolds transport theorem) will be used to integrate the equations of motion given in Eq. (3.8). A suitable form for the application in this section is (see also Fig. 21):

$$\frac{d}{dz}\int_0^{a(z)} s(r,z)dr = \int_0^{a(z)} \frac{\partial s(r,z)}{\partial z}dr + s(a,z)\left.\frac{\partial a}{\partial z}\right|_a . \tag{3.13}$$

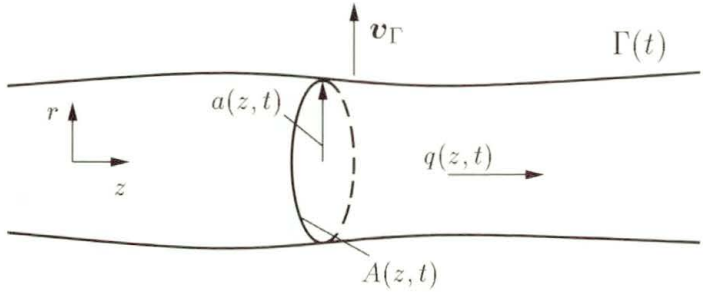

FIGURE 21. Flow $q(z,t)$ in a distensible tube with moving wall $\Gamma(t)$ and cross-sectional area $A(z,t)$.

Application to the second term of the continuity equation in Eq. (3.8) integrated over the radius:

$$2\pi\left[\int_0^{a(z)} \frac{1}{r}\frac{\partial}{\partial r}(rv_r)rdr + \int_0^{a(z)} \frac{\partial v_z}{\partial z}rdr\right] = 0 \tag{3.14}$$

yields:

$$2\pi\int_0^{a(z)} \frac{\partial rv_r}{\partial r}dr + 2\pi\frac{\partial}{\partial z}\int_0^{a(z)} v_z r dr - 2\pi v_z r\left.\frac{\partial a}{\partial z}\right|_a = 0 \tag{3.15}$$

or:

$$2\pi\, rv_r|_0^a + \frac{\partial q}{\partial z} - 2\pi v_z(a,t)a\left.\frac{\partial a}{\partial z}\right|_a = 0 \tag{3.16}$$

and thus:

$$2\pi a\left(v_r(a,t) - v_z(a,t)\left.\frac{\partial a}{\partial z}\right|_a\right) + \frac{\partial q}{\partial z} = 0 \tag{3.17}$$

with $q = q(z,t)$ the flow through the cross-section. Rewriting the first term in terms of the cross-sectional area $A(z,t) = \pi a^2(z,t)$, finally the integrated continuity equation reads:

$$\frac{\partial A}{\partial t} + \frac{\partial q}{\partial z} = 0. \tag{3.18}$$

This equation is formally derived but will be clear immediately from Fig. 21 if we write $[A(z,t+dt) - A(z,t)]dz + [q(z+dz,t) - q(z,t)]dt = 0$.

In a similar way the momentum equation in axial direction can be integrated:

$$2\pi \int_0^{a(z,t)} \frac{\partial v_z}{\partial t} r dr = -2\pi \int_0^{a(z,t)} \frac{1}{\rho}\frac{\partial p}{\partial z} r dr + 2\pi\nu \int_0^{a(z,t)} \frac{\partial}{\partial r}\left(r\frac{\partial v_z}{\partial r}\right) dr. \tag{3.19}$$

Application of the Leibnitz formulae to the first term yields:

$$2\pi \frac{\partial}{\partial t} \int_0^{a(z,t)} v_z r dr - 2\pi v_z v_r r|_0^a = -\frac{A}{\rho}\frac{\partial p}{\partial z} + 2\pi\nu r \left.\frac{\partial v_z}{\partial r}\right|_0^a. \tag{3.20}$$

The second term in the left hand side of this equation vanishes if a longitudinal restraint of the wall motion ($v_z(a) = 0$) is assumed. The second term in the right hand side can be written in terms of the wall shear stress defined in Eq. (2.25). The integrated momentum equation then reads:

$$\rho\frac{\partial q}{\partial t} + A\frac{\partial p}{\partial z} = -\frac{2A\tau}{a}. \tag{3.21}$$

Together with the expression for the wall shear stress given in Eq. (2.35) and linearisation of the $A\frac{\partial p}{\partial z}$ term we finally obtain:

$$\rho\frac{\partial q}{\partial t} + A_0\frac{\partial p}{\partial z} = -f_0 q \tag{3.22}$$

with f_0 a friction function defined as:

$$f_0(\omega) = i\omega\rho\frac{F_{10}(\omega)}{1 - F_{10}(\omega)}. \tag{3.23}$$

The linearized one-dimensional equations that describe the pressure and flow in distensible tubes under the assumption that $V/c \ll 1$, $(2\pi a/\lambda)^2 \ll 1$

and under the assumption that the wall motion is longitudinally constrained thus are given by:

$$\begin{cases} C_0 \dfrac{\partial p}{\partial t} + \dfrac{\partial q}{\partial z} = 0, \\ \rho \dfrac{\partial q}{\partial t} + A_0 \dfrac{\partial p}{\partial z} = -f_0 q, \end{cases} \tag{3.24}$$

with C_0 the linearized compliance given by:

$$C_0 = \left(\frac{\partial A}{\partial p} \right)_{p=p_0} \tag{3.25}$$

Alternatively using the mean velocity $\bar{v}$ instead of the flow $q = A\bar{v}$:

$$\begin{cases} D_0 \dfrac{\partial p}{\partial t} + \dfrac{\partial \bar{v}}{\partial z} = 0, \\ \rho \dfrac{\partial \bar{v}}{\partial t} + \dfrac{\partial p}{\partial z} = -f_0 \bar{v}, \end{cases} \tag{3.26}$$

with D_0 a linearized distensibility given by:

$$D_0 = \frac{1}{A_0} \left(\frac{\partial A}{\partial p} \right)_{p=p_0} \tag{3.27}$$

In the next section we will derive the wave number k for inviscid, viscosity dominated and general flow (i.e. large, small and intermediate values of the Womersley parameter α).

3.4.2. Wave speed and attenuation constant. The linearized one-dimensional mass and momentum equations for unsteady viscous flow through a distensible tube has been derived by integrating the continuity and momentum equations over a cross-section of the tube assuming the wave-length to be large compared to the diameter of the tube and the phase velocity of the wave to be large compared to the mean fluid velocity. Moreover it is assumed that the motion of the tube wall is restrained longitudinally. Due to the linearity assumed, the resulting Eqs. (3.18) and (3.22) can be solved in the frequency domain by substituting harmonic solutions

$$p(\omega, z, t) = \hat{p}(\omega, 0) e^{i(\omega t - kz)}, \tag{3.28}$$

$$q(\omega, z, t) = \hat{q}(\omega, 0) e^{i(\omega t - kz)}, \tag{3.29}$$

$$A(\omega, z, t) = \hat{A}(\omega, 0)e^{i(\omega t - kz)}, \tag{3.30}$$

where $\hat{p}(\omega, 0)$, $\hat{q}(\omega, 0)$ and $\hat{A}(\omega, 0)$ are the complex amplitudes representing both the amplitude and the phase of the waves measured at location $z = 0$, ω is the angular frequency and $k(\omega)$ is the wave number ; a complex number defined by:

$$k(\omega) = \frac{\omega}{c} - i\frac{\gamma(\omega)}{\lambda}. \tag{3.31}$$

Here c denotes the phase velocity of the waves and the wave length is given by $\lambda = 2\pi c/\omega$. The exponential decrease of the amplitude of the waves is described by the attenuation constant $\gamma(\omega) = -2\pi k_i/k_r$.

Viscoelastic wall behavior is described by an experimentally determined constitutive relationship between the cross-sectional area $\hat{A}$ and the complex amplitude $\hat{p}$:

$$\hat{A} = C(\omega)\hat{p} \tag{3.32}$$

where $C(\omega)$ is the dynamic compliance. For thin walled visco-elastic tubes this relationship can also be derived from Eqs. (1.3) using a complex Young's modulus $E = E_r + iE_i$.

Large Womersley number flow

For large Womersley parameters the flow will be inviscid and the friction function f_0 can be neglected. Substitution of Eqs. (3.28–3.30) in Eq. (3.24) yields:

$$\begin{cases} i\omega C(\omega)\hat{p} - ik(\omega)\hat{q} = 0, \\ \\ -ik(\omega)A_0\hat{p} + i\omega\rho\hat{q} = 0, \end{cases} \tag{3.33}$$

with solution:

$$k_0(\omega) = \pm\sqrt{\frac{\omega^2\rho C(\omega)}{A_0}} = \pm\frac{\omega}{c_0} \tag{3.34}$$

where the positive (negative) sign holds for waves traveling in the positive (negative) z-direction and c_0 denotes the Moens-Korteweg wave speed given by:

$$c_0(\omega) = \sqrt{\frac{A_0}{\rho C(\omega)}} = \sqrt{\frac{1}{\rho D_0(\omega)}}. \tag{3.35}$$

Note that the subscript $_0$ is used in k_0 and c_0 in order to obey conventions in literature despite the fact that k_∞ and c_∞ would be more meaningful

since $\alpha \to \infty$. For thin walled tubes the Moens-Korteweg wave speed can be derived from (1.3) and reads:

$$c_0 = \sqrt{\frac{1}{\rho} \frac{hE}{2a_0(1-\mu^2)}} \tag{3.36}$$

Note that the wave number $k_0 = \omega/c_0$ is a real number expressing that the phase velocity c equals the Moens-Korteweg wave speed and that the attenuation constant γ equals zero:

$$\alpha \to \infty : \qquad c(\omega) = c_0, \qquad \gamma(\omega) = 0. \tag{3.37}$$

As there is no friction and the compliance is assumed to be real (no visco-elasticity), no attenuation ($\gamma(\omega) = 0$) of the wave will occur. The corresponding wave equation can be derived from Eq. (3.24): after elimination of the flow and keeping in mind that the friction function is neglected we obtain the differential equation:

$$\frac{\partial^2 p}{\partial t^2} - \frac{1}{\rho D_0} \frac{\partial^2 p}{\partial z^2} = 0 \tag{3.38}$$

This is a wave equation with wave speed $c_0 = \sqrt{1/\rho D_0}$. So for large α and real values for the distensibility D_0 the pressure wave travels without damping in z-direction.

Equation (3.33) can also be solved with respect to the ratio $\hat{q}/\hat{p}$ between the flow and the pressure:

$$Y_0 = \frac{\hat{q}}{\hat{p}} = C(\omega) \frac{\omega}{k(\omega)} = \pm \frac{A_0}{\rho c_0}. \tag{3.39}$$

This ratio is referred to as the admittance Y_0 and is equal to the reciprocal value of the impedance:

$$Y \equiv \frac{1}{Z} \equiv \frac{\hat{q}}{\hat{p}}. \tag{3.40}$$

As $k(\omega)$ represents two waves (one wave traveling in positive z-direction ($k > 0$) and one wave traveling in negative z-direction ($k < 0$)) there are two flow and pressure waves: forward traveling waves $q_f = +Y p_f$ and backward traveling waves $q_b = -Y p_b$. The total pressure and flow is the sum of these waves $p(z,t) = p_f(z,t) + p_b(z,t)$ resp. $q(z,t) = q_f(z,t) + q_b(z,t)$.

Small Womersley number flow

For small Womersley parameters the flow will be dominated by viscous forces and the friction function f_0 can be approximated by its Poiseuille value $f_0 = 8\eta/a_0^2$ whereas the instationary inertia forces in the momentum equation can be neglected. Substitution of Eqs. (3.28–3.30) in Eq. (3.24) yields:

$$\begin{cases} i\omega C(\omega)\hat{p} - ik(\omega)\hat{q} = 0, \\ \\ -ik(\omega)A_0\hat{p} + \dfrac{8\eta}{a_0^2}\hat{q} = 0, \end{cases} \tag{3.41}$$

and has a non-trivial solution if:

$$k(\omega) = \pm\sqrt{\frac{-8i\eta\omega C(\omega)}{A_0 a_0^2}} = \pm\frac{\omega}{c_0}\sqrt{\frac{-8i}{\alpha^2}} = \pm\frac{2(1-i)}{\alpha}k_0 \tag{3.42}$$

where the positive (negative) sign now holds for waves traveling in the positive (negative) z-direction and c_0 denotes the Moens-Korteweg wave speed.

Now the wave number is a complex number and the phase velocity c and attenuation constant γ are given by:

$$\alpha \to 0: \qquad c(\omega) = \tfrac{1}{2}\alpha c_0, \qquad \gamma(\omega) = 2\pi. \tag{3.43}$$

As the real and imaginary part of the wave number are equal, the wave is damped critically. This can also be seen from Eq. (3.24): after elimination of the flow and keeping in mind that the instationary inertia forces can be neglected we obtain the differential equation:

$$\frac{\partial p}{\partial t} = \frac{A_0 a_0^2}{8\eta C_0}\frac{\partial^2 p}{\partial z^2} = \frac{a_0^2}{8\eta D_0}\frac{\partial^2 p}{\partial z^2}. \tag{3.44}$$

This is a diffusion equation with diffusion coefficient $D = a_0^2/8\eta D_0$. So for small α the wave equation reduces to a diffusion equation showing critical damping of the pressure in z-direction. This phenomena is responsible for the large pressure drop that is found in the micro-circulation where the Womersley parameter is low as a result of the small diameters of the vessels.

The admittance Y now is a complex number given by:

$$Y = \pm\frac{A_0}{\rho c_0}\frac{i+1}{4}\alpha = \frac{i+1}{4}\alpha Y_0. \tag{3.45}$$

Arbitrary Womersley number flow

Substitution of Eqs. (3.28–3.30), (3.32) and (3.23) in Eqs. (3.18) and (3.22) yields:

$$\begin{cases} i\omega C(\omega)\hat{p} - ik(\omega)\hat{q} = 0, \\ \\ -ik(\omega)A_0\hat{p} + (i\omega\rho + f_0)\hat{q} = 0. \end{cases} \tag{3.46}$$

After putting the determinant of the resulting set to zero the following expression for the wave number k is found:

$$k(\omega) = \pm\frac{\omega}{c_0}\sqrt{\frac{1}{1 - F_{10}(\omega)}} = \pm k_0\sqrt{\frac{1}{1 - F_{10}(\omega)}}\,. \tag{3.47}$$

Note that the wave number is again complex due to the friction function f_0 as defined in Eq. (3.23) or due to the visco-elasticity of the tube expressed in a complex value for the compliance $C(\omega)$. The phase velocity $c = \omega/k_r$ and attenuation constant $\gamma = -2\pi k_i/k_r = -\lambda k_i$ can be derived from Eq. (3.47) and are given in Fig. 22.

It has been mentioned that viscoelastic tubes will yield a complex compliance. From experiments it is shown that the viscous part of the modulus

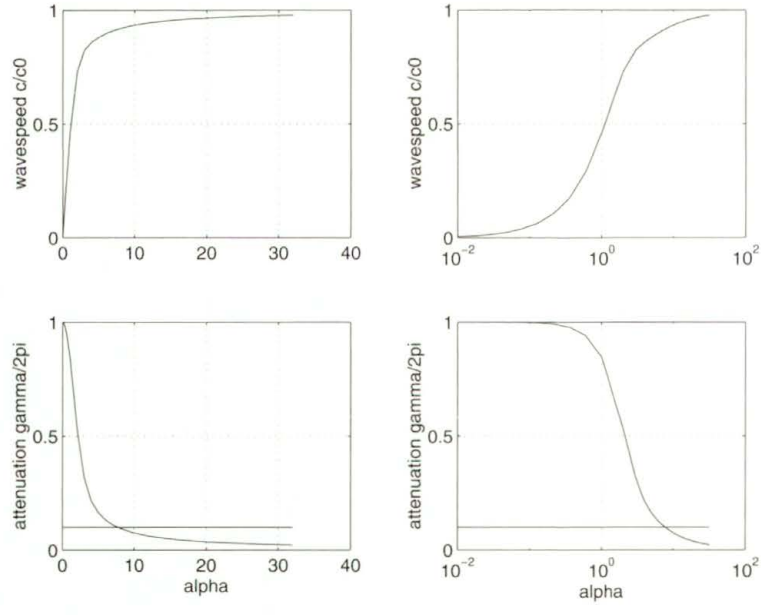

FIGURE 22. Phase velocity c/c_0 and attenuation constant $\gamma/2\pi$ as a function of α

is about 0.1 to 0.2 times the elastic part so $E = E_r(1+if_v)$ with the fraction $f_v \approx 0.15$. For large alpha the visco-elasticity then will give a imaginary part in the wave number according to:

$$k = \frac{\omega}{c_0}\frac{1}{\sqrt{1+if_v}} \approx k_0(1-\tfrac{1}{2}if_v). \tag{3.48}$$

This line is indicated in Fig. 22 and shows that for larger α (high frequencies and large arteries) the visco-elastic properties of the wall are the main cause for the attenuation of the pressure waves.

Finally the admittance can be derived as:

$$Y = \frac{k_0}{k}Y_0 \tag{3.49}$$

and is given in Fig. 23.

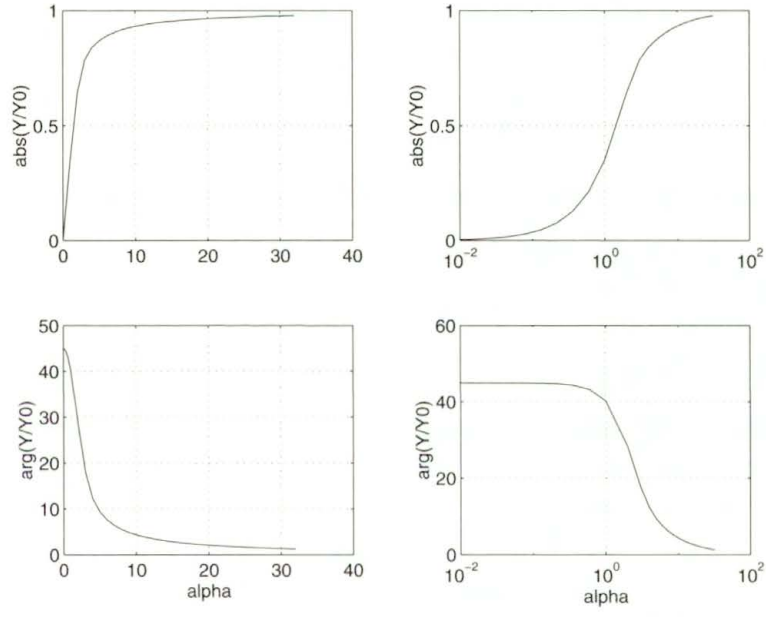

FIGURE 23. Absolute value and argument of Y/Y_0 as a function of α.

Propagation of a pressure pulse in homogeneous tubes

As an example in Fig. 24 the propagation of pressure waves in an elastic (left) and a visco-elastic (right) tube are computed. For this computation the following characteristic data for the carotid artery are used:

η	$3.5 \cdot 10^{-3}$	Pa·s	viscosity
a_0	$3 \cdot 10^{-3}$	m	radius
h	$a_0/10$	m	wall thickness
ρ	10^3	$\mathrm{kg \cdot m^{-3}}$	density of fluid
E	$4.5 \cdot 10^5$	$\mathrm{N \cdot m^{-2}}$	Young's modulus
μ	0.5	–	Poisson's ratio

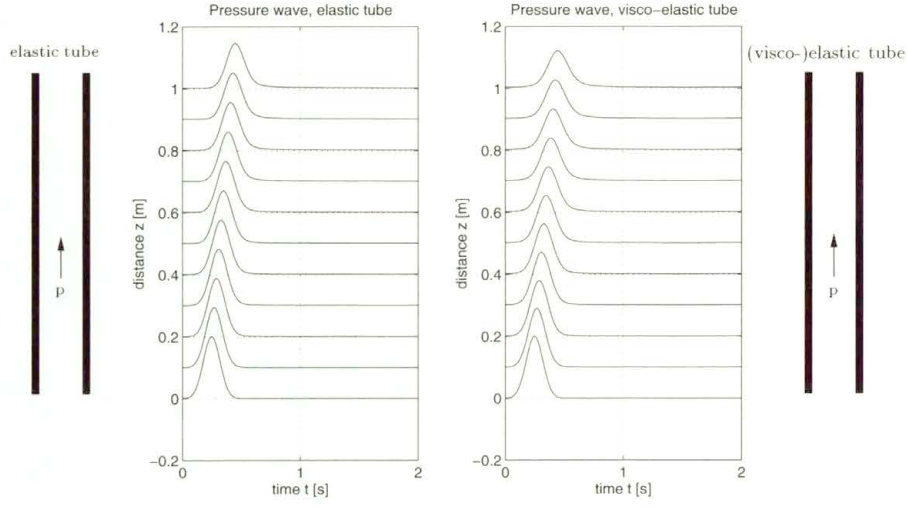

FIGURE 24. Propagation of pressure waves in an elastic tube (left) and a viscoelastic ($E = E(1 + i * 0.2)$) tube (right).

For the viscoelastic tube, the Young's modulus was taken to be $E(1+0.2i)$. Using Eq. (1.4) the distensibility and thus the compliance is determined. The wave number then was computed using Eqs. (3.47) and (3.35). The incident pressure pulse is given as:

$$p(0,t) = \exp\left(-\left(\frac{t-0.25}{0.1}\right)^2\right). \tag{3.50}$$

Clearly the damping of the wave due to viscous forces (i.e. wall shear stress) and viscoelastic properties of the wall can be distinguished.

3.5. Wave Reflection

3.5.1. Wave reflection at discrete transitions. We will refer to transitions which are highly compact as discrete transitions. In these cases the length of the transition is so small compared to the wave length of the waves

so that there is no difference in pressure or rate of flow between both ends of the transition, and the reflection phenomena can be described based on the equations of continuity of pressure and rate of flow across the transition. Figure 25 shows a discrete transition as might be formed by an increase or decrease in wall thickness at $z = L$. If the incident pressure and flow wave are represented by p_i and q_i respectively, the reflected waves by p_r and q_r, and the transmitted waves by p_t and q_t, continuity of pressure and rate of flow at a transition at location $z = L$ can be expressed as:

$$p_i(\omega, L, t) + p_r(\omega, L, t) = p_t(\omega, L, t), \tag{3.51}$$

$$q_i(\omega, L, t) + q_r(\omega, L, t) = q_t(\omega, L, t). \tag{3.52}$$

The ratio between a single traveling pressure wave and its corresponding flow waves is dependent on the impedance Z or admittance Y of the tube. An expression for the impedance or admittance can be obtained by substituting Eqs. (3.28–3.30) and (3.32) in Eq. (3.18):

$$Y(\omega) = \frac{1}{Z(\omega)} = \frac{\hat{q}(\omega, z)}{\hat{p}(\omega, z)} = \frac{\omega C(\omega)}{k(\omega)}. \tag{3.53}$$

Note that normally the admittance is defined for waves traveling in positive z-direction i.e. $k > 0$. In that case the flow amplitude is given by $\hat{q} = +Y\hat{p}$. For $k < 0$ the wave is traveling in negative z-direction and for an admittance defined for positive k we have a flow amplitude $\hat{q} = -Y\hat{p}$.

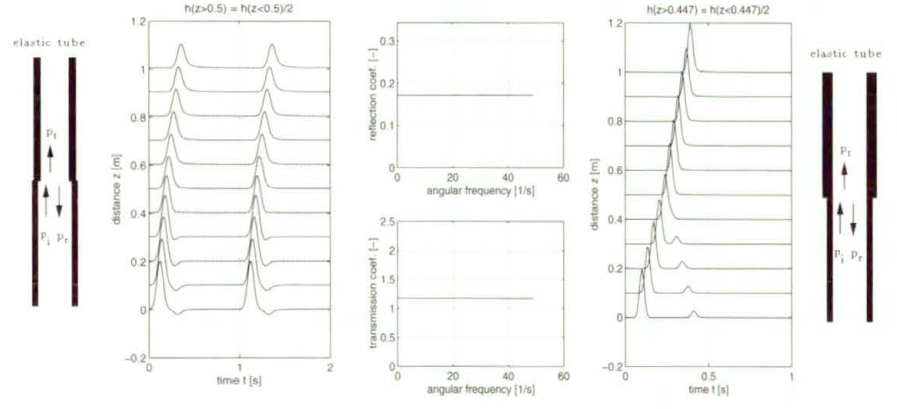

FIGURE 25. Wave reflection and propagation at discrete transitions formed by a sudden increase (left) and decrease (right) of the wall thickness.

Substitution of Eq. (3.53) in Eqs. (3.51) and (3.52) results in expressions for the reflection coefficient Γ_0 and the transmission coefficient T_{01}:

$$\Gamma_0(\omega) = \frac{\hat{p}_r(\omega, L)}{\hat{p}_i(\omega, L)} = \frac{Y_0(\omega) - Y_1(\omega)}{Y_0(\omega) + Y_1(\omega)}, \tag{3.54}$$

$$T_{01}(\omega) = \frac{\hat{p}_t(\omega, L)}{\hat{p}_i(\omega, L)} = \frac{2Y_0(\omega)}{Y_0(\omega) + Y_1(\omega)}, \tag{3.55}$$

where Y_0 is the admittance of the tube proximal to the transition, and Y_1 the admittance of the tube distal to the transition. The propagation of an incident wave $p_i = \hat{p}_i(\omega, 0)\exp(i(\omega t - k_0 z))$ in a tube with a discrete transition at $z = L$ can be expressed as:

$$\begin{cases} z < L: & \\ p(\omega, z, t) & = p_i(\omega, z, t) + p_r(\omega, z, t) \\ & = \hat{p}_i(\omega, 0) e^{-ik_0(\omega)z} \left[1 + \Gamma_0(\omega) e^{-2ik_0(\omega)(L-z)}\right] e^{i\omega t}, \\ z > L: & \\ p(\omega, z, t) & = p_t(\omega, z, t) \\ & = \hat{p}_i(\omega, 0) e^{-ik_0(\omega)L} T_{01}(\omega) e^{-ik_1(\omega)(z-L)} e^{i\omega t}. \end{cases} \tag{3.56}$$

As an example we consider the wave reflection of a transition formed by a sudden increase and a sudden decrease of the wall thickness ($h(z < L) = a/10$ while $h(z > L) = a/5$ and $h(z > L) = a/20$ respectively. The resulting wave propagation for $L = 0.5$ is given in Fig. 25.

From these figures it can be seen that a sudden decrease in wall thickness and thus a sudden increase of the distensibility or stiffness (Eh) of the wall leads to a negative reflection of the incident wave and a transmitted wave with a decreased pressure amplitude and a decreased wave speed. For a sudden decrease of the stiffness the opposite phenomena occur.

In a similar way as in equation (3.56) expressions can be obtained for the reflection and transmission coefficient of a bifurcation of uniform tubes (see Fig. 26) at $z = L$, here referred to as a discrete bifurcation. In that case continuity of pressure and flow yields:

$$p_i(\omega, L, t) + p_r(\omega, L, t) = p_{t_1}(\omega, L, t) = p_{t_2}(\omega, L, t), \tag{3.57}$$

$$q_i(\omega, L, t) + q_r(\omega, L, t) = q_{t_1}(\omega, L, t) + q_{t_2}(\omega, L, t), \tag{3.58}$$

resulting in:

$$\Gamma_0(\omega) = \frac{\hat{p}_r(\omega, L)}{\hat{p}_i(\omega, L)} = \frac{Y_0(\omega) - (Y_1(\omega) + Y_2(\omega))}{Y_0(\omega) + (Y_1(\omega) + Y_2(\omega))} \tag{3.59}$$

$$T_{01}(\omega) = \frac{\hat{p}_{t_1}(\omega, L)}{\hat{p}_i(\omega, L)} = \frac{2Y_0(\omega)}{Y_0(\omega) + (Y_1(\omega) + Y_2(\omega))} \tag{3.60}$$

$$T_{02}(\omega) = \frac{\hat{p}_{t_2}(\omega, L)}{\hat{p}_i(\omega, L)} = T_{01}(\omega). \tag{3.61}$$

Here p_{t_1} and p_{t_2} are the waves transmitted into the daughter tubes, and Y_1 and Y_2 are the impedances of these daughter tubes. Expressions for the pressure waves are similar to the ones given for the discrete transition in Eqs. (3.56).

In Fig. 26 the wave reflection caused by a bifurcation of a tube with radius a_0 into two tubes with respectively radius a_1 and a_2 is given for $a_0 : a_1 : a_2 = 1 : 1 : 1$ (left) and $a_0 : a_1 : a_2 = 3 : 2.1 : 1.8$ (right). One can observe a negative and a positive reflection of the incident wave due to the fact that $a_0^2 < a_1^2 + a_2^2$ and $a_0^2 > a_1^2 + a_2^2$ respectively and a wave speed which is slightly higher in the branch with the smallest radius.

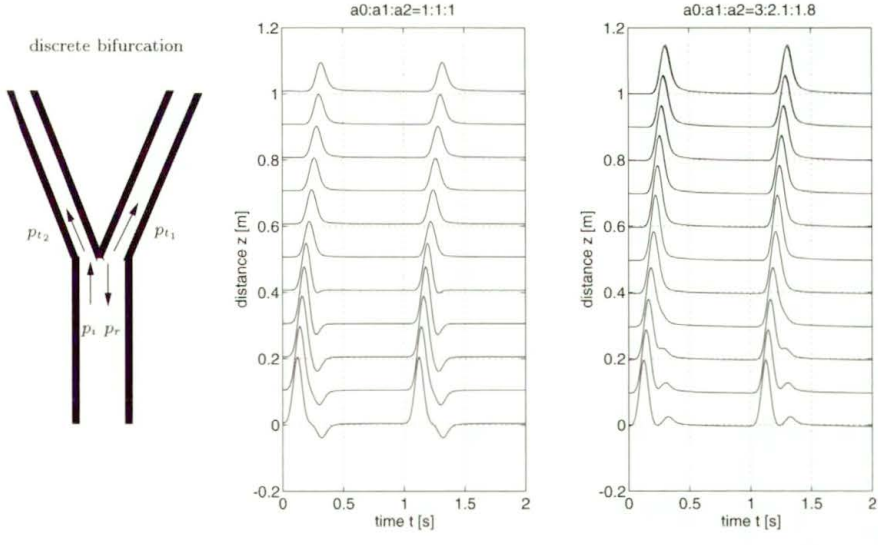

FIGURE 26. Wave reflection and propagation at a discrete bifurcation.

Note that the transmission and reflection coefficients given in Eqs. (3.54–3.55) and (3.59–3.61) are special cases of a general N-way junction with:

$$p_i(\omega, L, t) + p_r(\omega, L, t) = p_{t_j}(\omega, L, t), \qquad j = 1, \ldots, N, \tag{3.62}$$

$$q_i(\omega, L, t) + q_r(\omega, L, t) = \sum_{j=1}^{N} q_{t_j}(\omega, L, t), \tag{3.63}$$

resulting in:

$$\Gamma_0(\omega) = \frac{\hat{p}_r(\omega, L)}{\hat{p}_i(\omega, L)} = \frac{Y_0(\omega) - \sum\limits_{j=1}^{N} Y_j(\omega)}{Y_0(\omega) + \sum\limits_{j=1}^{N} Y_j(\omega)}, \tag{3.64}$$

$$T_{0j}(\omega) = \frac{\hat{p}_{t_j}(\omega, L)}{\hat{p}_i(\omega, L)} = \frac{2Y_0(\omega)}{Y_0(\omega) + \sum\limits_{j=1}^{N} Y_j(\omega)}, \qquad j = 1, \ldots, N. \tag{3.65}$$

3.5.2. Multiple wave reflection: effective admittance. Consider two N-way junctions at a distance L_{mn} apart from each other as given in Fig. 27.

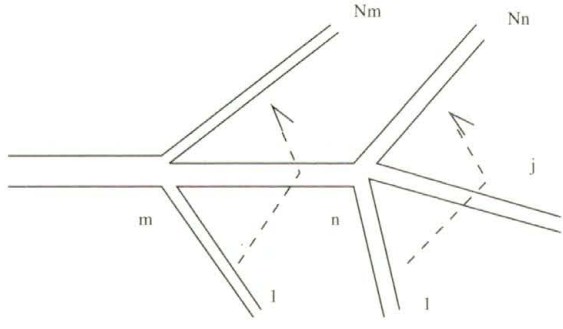

FIGURE 27. Multiple junctions.

At junction n we have:

$$\Gamma_n = \frac{Y_{mn} - \sum\limits_{j=1}^{N_n} Y_{nj}^e}{Y_{mn} + \sum\limits_{j=1}^{N_n} Y_{nj}^e}, \qquad T_{nj} = \frac{2Y_{mn}}{Y_{mn} + \sum\limits_{j=1}^{N_n} Y_{nj}^e}, \tag{3.66}$$

where Y^e_{nj} is the effective admittance of section nj at location n. If there are no reflected waves in section nj then $Y^e_{nj} = Y_{nj}$.

At junction m we have:

$$\Gamma_m = \frac{Y_m - \sum_{n=1}^{N_m} Y^e_{mn}}{Y_m + \sum_{n=1}^{N_m} Y^e_{mn}}, \qquad T_{mn} = \frac{2Y_m}{Y_m + \sum_{j=1}^{N_m} Y^e_{mn}}, \tag{3.67}$$

with:

$$Y^e_{mn} = \frac{\hat{q}(\omega, L_1)}{\hat{p}(\omega, L_1)} = Y_{mn} \frac{\exp(ik_{mn}L_{mn}) - \Gamma_n \exp(-ik_{mn}L_{mn})}{\exp(ik_{mn}L_{mn}) + \Gamma_n \exp(-ik_{mn}L_{mn})}. \tag{3.68}$$

In this way it is possible to compute the pressure and flow in a complete transmission line network, starting from a distal impedance going back to the aorta. An example of such a computation is given in Fig. 28 where the input impedance at the aorta is given as a function of the frequency. A minimum of $|Z|$ is found corresponding with a phase angle of zero. In [4] this is attributed to a reflection from the aorta bifurcation.

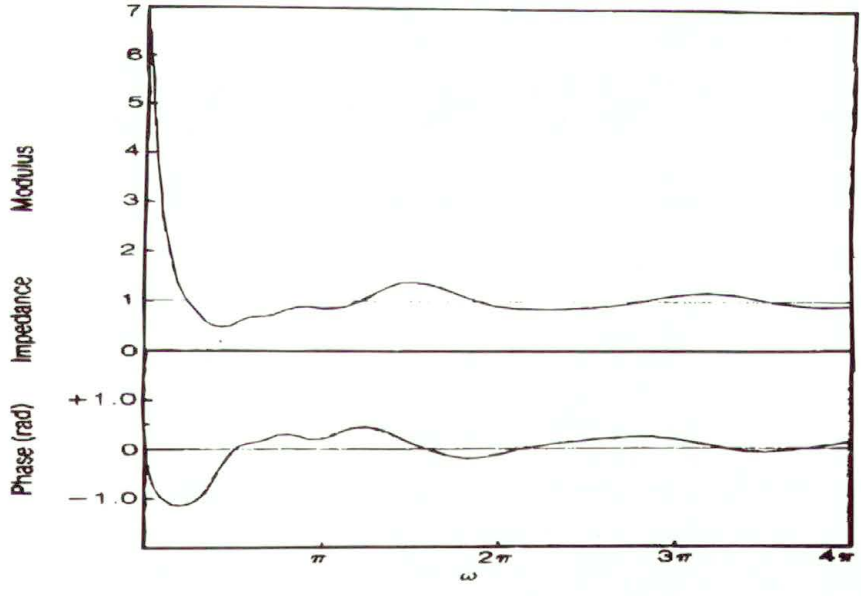

FIGURE 28. Input impedance at the aorta as a function of the frequency, after [4].

The reflection mentioned above can be explained from the expression we obtain after substitution of Eq. (3.66) in Eq. (3.68) yields:

$$Y^e_{mn} = Y_{mn} \frac{\sum_{j=1}^{N_n} Y^e_{nj} + iY_{mn} \tan(k_{mn}L_{mn})}{Y_{mn} + i \sum_{j=1}^{N_n} Y^e_{nj} \tan(k_{mn}L_{mn})} . \tag{3.69}$$

For $k_{mn}L_{mn} = 0, \pm\pi, \pm 2\pi, \ldots$ we find $Y^e_{mn} = \sum_{j=1}^{N_n} Y^e_{nj}$ and the section mn has no influence. These phenomena are illustrated in Fig. 29 showing the impedance Z^e_{mn}/Z_0 in a tube with characteristic impedance $Z_0 = Z_{mn}$ as a function of the frequency and distance from a termination with impedance $Z^e_T = 4Z_0$. Also the effect of attenuation is shown.

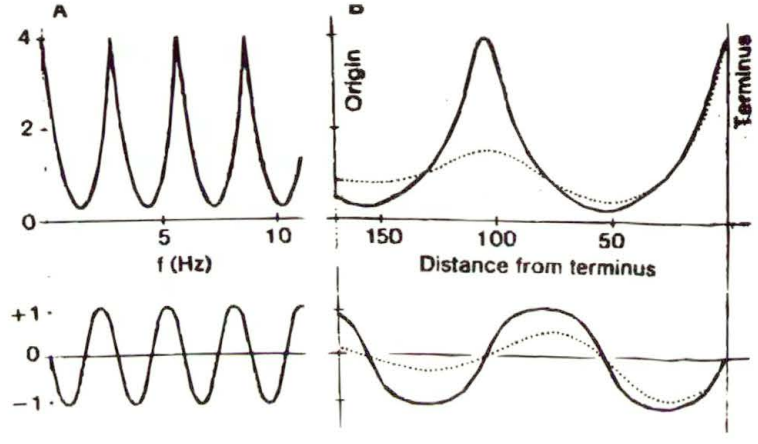

FIGURE 29. Effective impedance as a function of the frequency (left) and distance from termination (right) with (...) and without (–) attenuation, [4].

From expression (3.68) (or 3.69) we can see that for $k_{mn}L_{mn} \ll 1$ we simply have $\exp(\pm ikL) = 1$ and after substitution of Eq. (3.66):

$$Y^e_{mn} = Y_{mn} \frac{1 - \Gamma_n}{1 + \Gamma_n} = \sum_{j=1}^{N_n} Y^e_{nj} \qquad \text{if } k_{mn}L_{mn} \ll 1 \tag{3.70}$$

as if the section mn did not exist. If, however, $k_{mn}L_{mn}$ is small but still large enough that first order terms can not be neglected (i.e. $k^2_{mn}L^2_{mn} \ll 1$) we have:

$$Y^e_{mn} = Y_{mn} \frac{1 + ik_{mn}L_{mn} - \Gamma_n(1 - ik_{mn}L_{mn})}{1 + ik_{mn}L_{mn} + \Gamma_n(1 - ik_{mn}L_{mn})} \tag{3.71}$$

and after substitution of Eq. (3.66):

$$Y^e_{mn} = Y_{mn} \frac{ik_{mn}L_{mn}Y_{mn} + \sum_{j=1}^{N_n} Y^e_{nj}}{Y_{mn} + ik_{mn}L_{mn} \sum_{j=1}^{N_n} Y^e_{nj}} \qquad \text{if } k^2_{mn}L^2_{mn} \ll 1. \tag{3.72}$$

If we neglect terms of $\mathcal{O}(k^2L^2)$ we obtain:

$$Y^e_{mn} = \sum_{j=1}^{N_n} Y_{nj} + ik_{mn}L_{mn}Y_{mn} \left[1 - \left(\frac{\sum_{j=1}^{N_n} Y^e_{nj}}{Y_{mn}} \right)^2 \right]. \tag{3.73}$$

From this we can see that for intermediate long transitions only the phase of the admittance and not its absolute value is changed, [5].

So far, no attention was paid to reflections originating from peripheral vascular beds. However, these reflection phenomena might play an important role and can easily be taken into account. In the presence of reflected waves in the distal parts of a discrete transition, the reflection and transmission coefficient at an N-way junction read:

$$\Gamma_0(\omega) = \frac{Y_0 - \sum_{j=1}^{N} \frac{1-\Gamma^d_j}{1+\Gamma^d_j} Y_j}{Y_0 + \sum_{j=1}^{N} \frac{1-\Gamma^d_j}{1+\Gamma^d_j} Y_j}, \tag{3.74}$$

$$T_{0j}(\omega) = \frac{2Y_0}{Y_0 + \sum_{j=1}^{N} \frac{1-\Gamma^d_j}{1+\Gamma^d_j} Y_j}, \qquad j = 1, \ldots, N. \tag{3.75}$$

This result can directly be derived from the results for distal sections without reflection by replacing the admittance by its effective admittance using the reflection coefficients Γ^d_j of the distal sections at the junction (see 3.70). So the reflection from the distal vascular system is represented by the reflection coefficients Γ^d_j. These have to be determined from experimental data or can be estimated by modeling the distal part as a transition to an appropriate output impedance.

3.5.3. Vascular impedance and cardiac work. The importance of wave phenomena in the vascular system and the corresponding vascular impedance is clearly illustrated if we want to investigate the mechanical work done by the left ventricle. For each cardiac cycle this work is the integral over time of the pressure × flow product:

$$W = \int_{t_0}^{t_0+T} pqdt. \tag{3.76}$$

This integral consists of two parts. The first part is the steady flow power W_s which is determined by the resistance R_0 of the vascular system (mainly the peripheral resistance) defined as the ratio between the mean pressure and the mean flow $R_0 = p_0/q_0$. The second part is the oscillatory flow power W_0 following from Eq. (3.76) and the vascular impedance for each harmonic n ($Z_n = |Z_n| \exp(i\theta_n)$). So:

$$W = \tfrac{1}{2} \sum_{n=1}^{N} q_n^2 |Z_n| \cos\theta_n + q_0^2 R_0. \tag{3.77}$$

In [4] the following values can be found:

	$q_0^2 R_0$	$\sum_n$
left ventricle	1400	200
right ventricle	155	73

For the systemic circulation the contribution of the higher harmonics to the total work is relatively low. This is due to the fact that $\cos\theta_n \ll 1$. As the value of Z_n directly influences the work that has to be done by the heart, knowledge of the influence of age, medicine and other factors on the value of Z_n is of great clinical importance.

4. Summary

In this lecture a short introduction to cardiovascular fluid mechanics is given. A simple (windkessel) model has been derived based on the knowledge that the cardiovascular systems is characterized by an elastic part (large arteries) and a flow resitance (micro circulation) In this model it is ignored that the fluid mechanics of the cardiovascular system is characterized by

complex geometries and complex constitutive behavior of the blood and the vessel wall. The vascular system, however, is strongly bifurcating and time dependent (pulsating) three-dimensional entrance flow will occur. In the large arteries the flow will be determined by both viscous and inertia forces and movement of the nonlinear viscoelastic anisotropic wall may be of significant importance. In the smaller arteries viscous forces will dominate and non-Newtonian viscoelastic properties of the blood may become essential in the description of the flow field.

Flow patterns in rigid straight, curved and branched tubes have been treated. The velocity profiles of fully developed Newtonian flow in a straight circular tube can easily be derived by integration of the Navier-Stokes equations in cylindrical coordinates using superposition of harmonics of the pressure pulse. Apart from a scale factor for the pressure, only one single parameter, the Womersley number $\alpha = a\sqrt{\omega/\nu}$, determines the character of the flow. For large values of this parameter the flow is dominated by inertia and flat velocity profiles are found oscillating 90° out of phase with the pressure gradient. For low values of α the flow is dominated by viscous forces and a quasi static Poiseuille flow is found that is 180° out of phase with the pressure gradient. For arbitrary values of α the velocity profiles are solutions of Bessel's function and can be interpreted as a composition of a viscosity dominated flow in the boundary layer and an inertia dominated flow in the core. The thickness of the boundary layer appears to depend on α according to $\delta/a = O(\alpha^{-1})$.

The flow in curved tubes with curvature ratio δ differs from that in straight tubes because also centrifugal forces are of importance. Due to these centrifugal forces, the pressure gradients in the bulk flow are not in equilibrium with the flow in the viscous boundary layers and a secondary flow is induced, resulting in a strongly disturbed axial flow. A new dimensionless parameter, the Dean number, defined as $\mathrm{Dn} = (a/R_0)^{1/2}\mathrm{Re}$, determines the importance of this secondary flow. The main features of the flow in branched tubes strongly resemble those of the flow in curved tubes.

Finally, linearized wave equations that govern the pressure and flow traveling through the arterial system are derived. For large values of the Womersley parameter these equations yield the Moens-Korteweg wave speed. For small values of the Womersley parameter a diffusion equation can be derived expressing perfusion flow in small arteries. For intermediate (arbitrary) values of the Womersley parameter wave speed and admittance can be ex-

pressed in terms of those derived for the Moens-Korteweg waves. Reflection of waves at discrete transitions are derived from continuity of pressure and rate of flow and allow determination of multiple wave reflection and the definition of effective admittance in order to determine vascular impedance and cardiac work.

References

1. M. ABRAMOWITZ and I. STEGUN, *Handbook of Mathematical functions* Dover Publications Dover 1964
2. W.M. COLLINS and S.C.R. DENNIS, *The steady motion of a viscous fluid in a curved tube*, Q.J.Mech. Appl. Math **28**: 133–156, 1975
3. A.C. GUYTON, *Textbook of Medical Physiology*, Saunders 1967
4. W.R. MILNOR, *Hemodynamics*, Williams & Wilkins Baltimore, Hong Kong, London, Sidney 1989
5. T.J. PEDLEY, *The fluid mechanics of large blood vessels*, Cambridge University Press, Cambridge 1980
6. H. SCHLICHTING, *Boundary Layer Theory*, McGraw-Hill, New York 1960
7. A.J. WARD-SMITH, *Internal fluid flow*, Oxford 1980
8. J.R. WOMERSLEY, *The mathematical analysis of the arterial circulation in a state of oscillatory motion*, Technical report wadc-tr-56-614, Wright Air Development Center 1957